Open access • Journal Article • DOI:10.2514/3.44681

Effect of tip vortex structure on helicopter noise due to blade-vortex interaction

Sheila E. Widnall, Thomas L. Wolf

Institutions: Massachusetts Institute of Technology

Published on: 01 Oct 1980 - Journal of Aircraft (American Institute of Aeronautics and Astronautics (AIAA))

Topics: Vortex ring, Starting vortex, Vortex lift, Horseshoe vortex and Vortex

CR-152150

M.I.T. Fluid Dynamics Research
Laboratory Report 78-2

THE EFFECT OF TIP VORTEX STRUCTURE ON HELICOPTER NOISE DUE TO BLADE/VORTEX INTERACTION

Thomas L. Wolf

and

Sheila E. Widnall

MASSACHUSETTS INSTITUTE OF TECHNOLOGY

FLUID DYNAMICS RESEARCH LABORATORY

March 1978

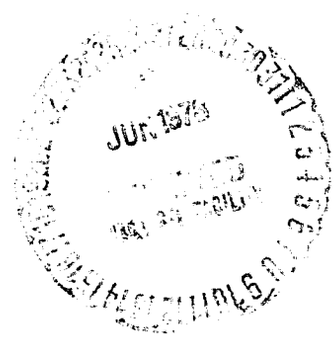

National Aeronautics and Space Administration
Ames Research Center
Moffett Field, California 94035
Contract Number: NSG-2142

THE EFFECT OF TIP VORTEX STRUCTURE ON HELICOPTER NOISE DUE TO BLADE/VORTEX INTERACTION

by

THOMAS L. WOLF

and

SHEILA E. WIDNALL

ABSTRACT

A potential cause of helicopter impulsive noise, commonly called blade slap, is the unsteady lift fluctuation on a rotor blade due to interaction with the vortex trailed from another blade. The relationship between vortex structure and the intensity of the acoustic signal is investigated. The analysis is based on a theoretical model for blade/vortex interaction, due originally to Widnall. Unsteady lift on the blades due to blade/vortex interaction is calculated using linear unsteady aerodynamic theory, and expressions are derived for the directivity, frequency spectrum, and transient signal of the radiated noise. The inviscid rollup model of Betz is used to calculate the velocity profile in the trailing vortex from the spanwise distribution of blade tip loading. A few cases of tip loading are investigated, and numerical results are presented for the unsteady lift and acoustic signal due to blade/vortex interaction. The intensity of the acoustic signal is shown to be quite sensitive to changes in tip vortex structure.

TABLE OF CONTENTS

Chapter No.		Page
1	INTRODUCTION	6
2	UNSTEADY AERODYNAMICS OF BLADE/VORTEX INTERACTION	10
3	ACOUSTIC RADIATION FROM BLADE/VORTEX INTERACTION	14
4	THE BETZ VORTEX MODEL	28
5	APPLICATION TO A NUMERICAL SCHEME	31
6	RESULTS AND DISCUSSION	33
7	CONCLUSIONS	42

Appendices

A	SOUND FIELD DUE TO A CONVECTED POINT DIPOLE	44
B	LIFT TRANSFER FUNCTION OF FILOTAS THEORY	49
C	COMPUTER PROGRAM	50

Figures 65

REFERENCES 94

LIST OF SYMBOLS

b_o	reference length, blade semichord
C_L	unsteady section lift coefficient
c	speed of sound
D	directivity function, eqn. (3.27)
h	nondimensional distance; vortex to blade in semichords
k	nondimensional acoustic wavenumber $b_o\omega/c$
k_x, k_y	wavenumber in x, y direction
L_o	lift/unit span
M	blade normal Mach number; U/c
p	pressure
P	Fourier transform of the pressure
r	$= (x^2 + y^2 + z^2)$, also radial coordinate in trailing vortex
$\tilde{S}$	Strouhal frequency, $\tilde{S} = \tilde{\omega} b_o/U$
S	Doppler shifted Strouhal frequency
s_o	blade interaction length in semichords
t'	retarded time, eqn. (2.3)
U_c	convection velocity along the blade
U	blade velocity
v_θ	circumferential velocity in trailing vortex
w_o	vertical velocity as a function of ξ, fig. 3
W_o	Fourier transform of vertical velocity in wavenumber σ
w	vertical velocity as a function of t'
W	Fourier transform of vertical velocity in frequency $\tilde{S}$

x,y,z	Cartesian coordinate system, y also spanwise coordinate of chapter 4
α	angular velocity of the rotor (radians/second)
Γ_b	bound circulation on the blade (chapter 4)
Γ_v	circulation in the trailing vortex (chapter 4)
δ	delta function
Λ	angle between blade and vortex, fig. 3
ρ	fluid density
σ	wavenumber of Fourier transform in ξ , fig. 3
θ,ψ	coordinate system of fig. 4
$\tilde{\omega}$	aerodynamic frequency (radians/second)
ω	acoustic frequency (radians/second)
Ω	blade passage frequency (radians/second)

INTRODUCTION

The sound generated by a helicopter rotor can be categorized as either "rotational" or "broadband" noise. Rotational noise is characterized by a periodic acoustic signal giving rise to line spectra at the blade passage frequency and its harmonics. Broadband noise is nonharmonic and has a continuous spectrum.

Rotor noise is due to the combined effect of several complex acoustic mechanisms.[1] Sources of rotational noise include steady and periodic blade loading, and at sufficiently high blade Mach numbers, volume displacement and nonlinear aerodynamic effects. Broadband noise arises from randomly varying blade forces, due for example to atmospheric turbulence.

Under certain flight conditions, helicopter rotor operation produces an impulsive, highly directional noise, repeated at the blade passage frequency. Commonly referred to as "blade slap," it is the predominant acoustic effect when present. At least two mechanisms can be responsible for blade slap. One is shock formation due to local transonic flow on the advancing blade side. Another is the unsteady lift fluctuation on a blade caused by interaction with the tip vortex trailed from another blade. This blade/vortex interaction is the subject of the present investigation.

A rotor blade leaves behind a continuous vortex sheet due to spanwise lift variation. The inboard sheet is diffuse and does not seem to induce appreciable velocities at the rotor disc, while the more intense outboard sheet rolls up and moves inboard, forming a concentrated tip vortex (fig. 1). If flight conditions are such as to cause the rotor blades to pass in close proximity to these tip vortices, blade slap can occur.

Fig. 2 depicts schematically the loci of tip vortices and important blade/vortex interactions for single and tandem rotors. As indicated by the sketch, the essence of the blade/vortex interaction problem is that of a long blade passing obliquely over a vortex. For the case of small angles between the blade and vortex, the interaction occurs over a significant portion of the blade span, so that two-dimensional aerodynamics can be used to model the problem except near the blade tip. Comparison of figs. 2a and 2b indicates that blade/vortex interactions are more likely to occur at small angles for the case of the tandem rotor, although recent experimental evidence [2] indicates that such interactions can be an important source of noise for single rotor helicopters as well.

Widnall [3] has developed a theoretical model for blade/vortex interaction. The unsteady spanwise lift distribution is computed on a two dimensional airfoil passing obliquely over an infinite line vortex. This lift distribution is then taken as the boundary condition on a finite blade in the calculation of the acoustic farfield. The Widnall model has since been refined by Chu [4] in order to incorporate sweep and convective fluid ef ects.

In Widnall's original investigation, the tip vortex is modelled as a potential vortex. The viscous core is taken into account by locating the center of the vortex an "effective distance" below the blade, defined by

$$h_{eff} = \sqrt{h^2_{actual} + r^2_{core}}$$

where r_{core} is the radius of the vortex core.

The potential vortex model is convenient in that it affords an essentially analytical treatment of the problem. It gives good agreement

with experiment for square tipped blades. For the case of the blade cutting through the vortex core, experimental results show a plateauing of both pressure fluctuation on the blade and radiated noise. This effect is accurately predicted by the theory, provided r_{core} has been selected appropriately.

In the present study we examine the relationship between vortex structure and the acoustic pulse, in an attempt to identify features of the tip vortex that make the most damaging contribution to the radiated noise level. We have developed a numerical analogue of Widnall's analysis to compute the unsteady lift on the blade and the farfield acoustic signal associated with a vortex of arbitrary vorticity distribution.

We are also interested in predicting vortex structure given the distribution of blade loading, so that we can directly relate rotor blade design characteristics to acoustic performance. Recently this problem has received considerable attention in the study of aircraft wake turbulence, where attempts have been made to predict the trailing vortex structure in the wake of an arbitrarily loaded aircraft wing. Donaldson [5] has shown that the long forgotten model of Betz [6] can be successfully applied to the problem. Betz assumes that the circulation and moment of vorticity of the initially flat trailing vortex sheet are conserved during the rollup process, and derives a relationship between the spanwise coordinate in the flat wake and the radial coordinate in the fully rolled up trailing vortex.

Donaldson shows that complicated spanwise loading configurations generate a discrete set of trailing vortices, such that each segment of the distribution contained between relative maxima or minima in the loading rolls

up into a single trailing vortex. Although helicopter blade loading fluctuates widely during flight, the position of maximum loading can be roughly estimated at 75% of blade span.[7] The loading falls off monotonically to zero at the blade tip. Hence, we need only consider the outer 25% of blade span in the determination of tip vortex structure. We assume that the tangential blade velocity is uniform over this length.

The Betz model is easily adapted to a numerical scheme. We apply it here to a few different loading configurations, holding the location and magnitude of the maximum blade loading constant for all cases. The choice of loading configurations is somewhat arbitrary, as little is known about the precise distribution of tip loading on helicopter blades. The examples have been selected to illustrate salient features of the model and to suggest general guidelines for design to minimize noise.

Finally, we discuss some general aspects of noise generation due to blade/vortex interaction and recent experimental attempts to minimize blade slap through tip shape modification. [2, 8]

2. UNSTEADY AERODYNAMICS OF BLADE/VORTEX INTERACTION

We wish to compute the unsteady lift distribution on a two dimensional airfoil passing obliquely over an infinite vortex filament. From linear aerodynamic theory, this unsteady lift can be calculated by requiring the condition of no flow through the airfoil in the presence of the upwash field induced by the vortex.

2.1 The Upwash Spectrum Due to Blade/Vortex Interaction

The geometry of blade/vortex interaction is depicted in fig. 3. Blade/vortex separation is h, angle of obliqueness Λ. As is standard in unsteady aerodynamics, all quantities have been nondimensionalized by the blade velocity U and blade semichord b_o. The coordinates are fixed in the fluid.

We define the spatial coordinate ξ measured perpendicular to the vortex in the plane of the airfoil. Then given the distribution of circumferential velocity in the vortex, along with h and Λ, the upwash induced at the airfoil location at a given instant can be written as $w_o(\xi)$. Using Fourier transforms, $w_o(\xi)$ is represented as a distribution, in spatial wavenumber σ, of sinusoidal gusts.

$$w_o(\xi) = \int_{-\infty}^{\infty} W_o(\sigma) e^{i\sigma\xi} d\sigma$$

$$W_o(\sigma) = \frac{1}{2\pi}\int_{-\infty}^{\infty} w_o(\xi) e^{-i\sigma\xi} d\xi \qquad (2.1)$$

As the blade passes over the vortex, the upwash pattern is convected along the span with nondimensional convection speed U_c, given by

$$U_c = \frac{1}{\tan \Lambda} \tag{2.2}$$

This upwash can be written as $w(t')$, where t' is the "retarded time" defined by

$$t' = t - \frac{x}{U_c} \tag{2.3}$$

We define the nondimensional aerodynamic frequency

$$\tilde{S} = \frac{\tilde{\omega} b_o}{U} \quad \text{, the Strouhal number.} \tag{2.4}$$

Here we have used the symbol '~' in order to distinguish the aerodynamic frequency from the acoustic frequency that appears in Chapter 3.

Using Fourier transforms, the unsteady upwash $w(t')$ is represented as a distribution of sinusoidal gusts of frequency $\tilde{S}$.

$$\begin{aligned} w(t') &= \int_{-\infty}^{\infty} W(\tilde{S}) e^{i\tilde{S}t'} d\tilde{S} \\ W(\tilde{S}) &= \frac{1}{2\pi} \int_{-\infty}^{\infty} w(t') e^{-i\tilde{S}t'} dt' \end{aligned} \tag{2.5}$$

We can use eqns 2.1 to express the upwash spectrum, $W(\tilde{S})$ of eqns 2.5, in terms of the spatial upwash distribution $w_o(\xi)$. An airfoil passing over a sinusoidal gust of spatial wavenumber experiences velocity fluctuations of frequency

$$\tilde{S} = \sigma \cos \Lambda \tag{2.6}$$

From geometry,

$$t' = \frac{\xi}{\cos\Lambda} \tag{2.7}$$

These relations are substituted into eqns. (2.5) to give tne upwash spectrum,

$$W(\tilde{S}) = \frac{1}{2\pi}\int_{-\infty}^{\infty} w_o(\xi)e^{-i\sigma\xi}d\xi\left(\frac{1}{\cos\Lambda}\right) = \frac{1}{\cos\Lambda}W_o(\sigma) \tag{2.8}$$

$$\text{for } \sigma = \frac{\tilde{S}}{\cos\Lambda}$$

2.2 Unsteady Lift Due to Blade/Vortex Interaction

A gust of frequency $\tilde{S}$ causes a sinusoidal lift variation along the span

$$L(x,t;\tilde{S}) = L_o(\tilde{S},\Lambda)e^{i(k_x x-\tilde{S}t)} = L_o(\tilde{S},\Lambda)e^{-i\tilde{S}t'} \tag{2.9}$$

where $L_o(\tilde{S},\Lambda)$ is an (as yet) undetermined complex lift amplitude. Since the purpose of this work is to determine the effects of tip vortex structure upon the acoustic signature, we have used the incompressible theory of Filotas [9] to calculate the unsteady lift due to one such oblique sinusoidal gust. Compressibility effects are thereby excluded for reasons of simplicity and consistency with ref. 3. It is felt that these effects would not essentially alter the results of the present study. We are currently using the more complex unsteady aerodynamic theory of Amiet [15] to investigate the acoustic ratiation from blade/vortex interaction at higher frequencies in a compressible flow.

The Filotas theory gives the unsteady lift due to an oblique sinusoidal gust as

$$L(x,t,\tilde{S}) = \rho U^2 b_o C_L$$

$$C_L = 2\pi\alpha T$$

$$\alpha = W(\tilde{S})e^{i(k_x x - \tilde{S}t)} \qquad (2.10)$$

where α is the instantaneous angle of attack,

and $T = T(\sigma,\Lambda) = T(\frac{\tilde{S}}{\cos\Lambda},\Lambda)$ is the (complex) "lift transfer function" of Filotas, given in Appendix B.

T relates the magnitude and phase of the unsteady lift to that of the incident sinusoidal gust, analogous to the well known Sears' function for the case of a parallel blade/gust interaction. T=1 at zero reduced frequency (steady upwash case). As frequency tends to infinity, T approaches zero as the infinite number of upwash oscillations become mutually self-cancelling over the chord of the airfoil.

Comparing eqns (2.10) and (2.9), we have for the (complex) unsteady lift amplitude

$$L_o(\tilde{S},\Lambda) = 2\pi\rho U^2 b_o T(\frac{\tilde{S}}{\cos\Lambda},\Lambda)W(\tilde{S}) \qquad (2.11)$$

The unsteady lift at a spanwise station x is found by integrating eqn (2.9) over all frequencies, as the inverse Fourier transform

$$L(t') = \int_{-\infty}^{\infty} L_o(\tilde{S},\Lambda)e^{-i\tilde{S}t'}d\tilde{S} \qquad (2.12)$$

For reference, we include the forward transform

$$L_o(\tilde{S},\Lambda) = \frac{1}{2\pi}\int_{-\infty}^{\infty} L(t')e^{i\tilde{S}t'}dt' \qquad (2.13)$$

3. ACOUSTIC RADIATION FROM BLADE/VORTEX INTERACTION

We now analyze the acoustic field due to blade/vortex interaction. The unsteady spanwise lift distribution previously calculated is now taken as a boundary condition on a blade of finite length in the solution of the acoustic wave equation.

3.1 Problem Formulation

We assume that the blade chord is smaller than a wavelength, so that the unsteady lift may be modelled as a line of acoustic dipoles, moving with velocity U in the y direction (fig. 4).

The governing equation for the unsteady pressure is

$$\nabla^2 p = \frac{1}{c^2}\frac{\partial^2 p}{\partial t^2} \tag{3.1}$$

Defining an effective blade/vortex interaction length s_0, the boundary condition may be written

$$\begin{aligned} p^-(x,y,0) - p^+(x,y,0) &= L(t-x/U_c)\delta(y-Ut) \quad |x| \leq s_0 \\ &= 0 \qquad\qquad\qquad\quad |x| > s_0 \end{aligned} \tag{3.2}$$

Dimensional variables have been introduced temporarily for the sake of clarity. $L(t-x/U_c)$ is the unsteady lift of eqn. (2.12), with U_c the phase velocity with which the lift pattern is convected along the blade, from eqn. (2.2).

Returning to a nondimensional formulation with reference quantities blade velocity U and semichord b_o, this boundary condition is written

$$p^-(x,y,0) - p^+(x,y,0) = L(t-x/U_c)\delta\{b_o(y-t)\} \quad |x| \leq s_o$$
$$= 0 \qquad\qquad |x| > s_o \tag{3.3}$$

where the dimensions of pressure p-force/length^2 and section lift L-force/length have been retained.

3.2 Transforming the Problem

We introduce the Fourier transform in x, y, and t, defining the transform pair

$$p(x,y,z,t) = \frac{1}{(2\pi)^3} \iiint_{-\infty}^{\infty} P(k_x,k_y,S;z)e^{ik_x x + ik_y y - iSt}\, dk_x dk_y dS \tag{3.4}$$

$$P(k_x,k_y,S;z) = \iiint_{-\infty}^{\infty} p(x,y,z,t)e^{-ik_x x - ik_y y + iSt}\, dxdydt$$

where S is nondimensional frequency, $\frac{\omega b_o}{U}$.

The Fourier transform of the boundary conditions is given by

$$\Delta P(k_x,k_y,S) = \int_{-\infty}^{\infty}\int_{-s_o}^{s_o} L(t-x/U_c)\delta\{b_o(y-t)\}\, e^{-ik_x x - ik_y y + iSt}\, dxdydt \tag{3.5}$$

From the properties of the delta function, the only contribution to the y-integral occurs at y=t. Using

$$\int_{-\infty}^{\infty} \delta(au)du = \frac{1}{a},$$

we perform the y integration.

$$\Delta P(k_x,k_y,S) = \int_{-\infty}^{\infty}\int_{-s_o}^{s_o} \frac{1}{b_o} L(t-x/U_c)\, e^{-ik_x x - ik_y y + iSt}\, dxdt \qquad (3.6)$$

To evaluate the t integral, we introduce the retarded time t', as in eqn. (2.3).

$$t' = t - \frac{x}{U_c}$$

dt' = dt (x is held constant over the t integration)

so that

$$\Delta P(k_x,k_y,S) = \int_{-\infty}^{\infty}\int_{-s_o}^{s_o} L(t')e^{-ik_x x}\, e^{i(S-k_y)(t'+x/U_c)}\, dxdt' \qquad (3.7)$$

Regrouping,

$$\Delta P(k_x,k_y,S) = \int_{-s_o}^{s_o} e^{i\{[(S-k_y)/U_c]-k_x\}x} \left\{\int_{-\infty}^{\infty} L(t')e^{i(S-k_y)t'}\, dt'\right\} dx \qquad (3.8)$$

The bracketed term in eqn. (3.8) is the Fourier transform of the unsteady lift in the frequency parameter $S-k_y$. With reference to

eqn. (2.13), we therefore identify $S-k_y$ as the aerodynamic frequency $\tilde{S}$, giving the transform of the unsteady lift as the unsteady lift spectrum $L_o(\tilde{S})$ (within a factor of 2π). Since P is the Fourier transform of the acoustic signal, we see that a Fourier component of unsteady lift of frequency $\tilde{S}$ on the moving boundary will be perceived at acoustic frequency S in the sound field. This is usually referred to as the Doppler shift.

Eqn. (3.8) then becomes

$$\Delta P(k_x,k_y,S) = 2\pi L_o(\tilde{S}) \int_{-s_o}^{s_o} e^{i(\tilde{S}/U_c - k_x)x} dx \qquad (3.9)$$

The x integration is straightforward, giving the Fourier transform of the boundary condition as

$$\Delta P(k_x,k_y,S) = \frac{4\pi}{b_o} L_o(\tilde{S}) \frac{\sin\{s_o(\tilde{S}/U_c - k_x)\}}{(\tilde{S}/U_c - k_x)} . \qquad (3.10)$$

We now take the Fourier transform of eqn. (3.1), giving

$$\frac{d^2P}{dz^2} - (k_x^2 + k_y^2 - k^2)P = 0 \qquad (3.11)$$

where the relation k=S/c has been used.

The solution to eqn. (3.11) is written

$$P(k_x,k_y,S) = A(k_x,k_y,S)e^{\pm z\sqrt{k_x^2+k_y^2-k^2}} \qquad (3.12)$$

where A can be complex.

The argument of the exponential in eqn. (3.12) must be purely complex for waves that are radiated into the farfield. This establishes as a cutoff condition

$$k^2 > k_x^2 + k_y^2 \text{ for non decaying waves} \tag{3.13}$$

From geometry $k_z = \sqrt{k^2-k_x^2-k_y^2}$, so that eqn (3.12) can be written

$$P(k_x,k_y,S) = A(k_x,k_y,S)e^{\pm ik_z z} \tag{3.14}$$

Considering only those waves that propagate outward from the boundary, so that the quantity $\pm k_z z$ is always positive, we define

$$\begin{aligned} &\text{for } z > 0, \quad P^+ = A^+ e^{i\sqrt{k^2-k_x^2-k_y^2}\, z} \\ &\text{for } z < 0, \quad P^- = A^- e^{-i\sqrt{k^2-k_x^2-k_y^2}\, z} \end{aligned} \tag{3.15}$$

We now impose the transformed boundary condition of eqn. (3.10).

$$P^- - P^+\Big|_{z=0} = \frac{4\pi}{b_o} L_o(\tilde{S}) \frac{\sin\{s_o(\tilde{S}/U_c - k_x)\}}{(\tilde{S}/U_c - k_x)}$$

In addition, we require that the pressure discontinuity be symmetric across the boundary, that is

$$\frac{\partial p^+}{\partial z} = \frac{\partial p^-}{\partial z}\Big|_{z=0}, \tag{3.16}$$

leading to $A^+ = -A^-$.

Application of these two boundary conditions determines the constants A^+ and A^-, giving the Fourier transform of the pressure as

$$P^{\pm}(k_x,k_y,S) = \mp \frac{2\pi}{b_o} L_o(\tilde{S}) \frac{\sin\{s_o(\tilde{S}/U_c - k_x)\}}{(\tilde{S}/U_c - k_x)} \tag{3.17}$$

Taking the inverse transform defined by eqns. (3.4) gives the pressure field as

$$p(x,y,z,t) = \frac{-1}{(2\pi)^2 b_o} \iiint_{-\infty}^{\infty} L_o(\tilde{S}) \frac{\sin\{s_o(\tilde{S}/U_c - k_x)\}}{(\tilde{S}/U_c - k_x)} e^{iz\sqrt{k^2-k_x^2-k_y^2}} e^{ik_x x + ik_y y - iSt} dk_x dk_y dS \tag{3.18}$$

3.3 Evaluating the Farfield Pressure

The pressure in the farfield is obtained by performing the integrations indicated in eqn. (3.18) in the limit of $\sqrt{x^2+y^2+z^2} \to \infty$. We take advantage of the farfield asymptotic behavior of the integrand to carry out the integrations over k_x and k_y, using the method of stationary phase [10].

In general the method of stationary phase utilizes the self cancelling oscillation of an exponential factor in an integrand, allowing the contribution of the integrand to be neglected everywhere except in the neighborhood of one or more critical points.

We identify the "phase" of the integrand in eqn. (3.18) as

$$\phi = z\{k_x \frac{x}{z} + k_y \frac{y}{z} + \sqrt{k^2 - k_x^2 - k_y^2}\} \tag{3.19}$$

If the phase is a rapidly increasing or decreasing function of k_x or k_y, the exponential $e^{i\phi}$ alternates rapidly in sign with a change in k_x or k_y. In the limit of $x,y,z \to \infty$, these oscillations become mutually self cancelling, so that contributions to the integral occur only in the vicinity of those points at which the phase is rendered "stationary" with respect to k_x and k_y. That is,

$$\frac{\partial \phi}{\partial x} = \frac{\partial \phi}{\partial y} = 0 \tag{3.20}$$

Application of eqns. (3.20) leads to the result

$$\begin{aligned} k_x^* &= k\frac{x}{r} \\ k_y^* &= k\frac{y}{r} \end{aligned} \tag{3.21}$$

where asterisks have been used to identify k_x and k_y evaluated at the stationary point.

From geometry, k_x^* and k_y^* describe a wave that propagates radially outward from a point source. Physically, the method of stationary phase tells us that only these waves are present in the farfield limit.

Whitham [11] presents the result for application of the method of stationary phase to multiple integrations. If we write eqn.(3.18) in the form

$$p(x,y,z,t) = \int_{-\infty}^{\infty}\int\int\int F(k_x,k_y,\tilde{S})e^{-izW} e^{ik_x x+ik_y y-iSt} dk_x dk_y dS \tag{3.22}$$

where

$$F(k_x,k_y,\tilde{S}) = \frac{-1}{(2\pi)^2} b_o L_o(\tilde{S}) \frac{\sin\{s_o(\tilde{S}/U_c - k_x)\}}{(\tilde{S}/U_c - k_x)}$$

and $$W(k_x,k_y,k) = -\sqrt{k^2 - k_x^2 - k_y^2}$$

then application of Whitham's formula leads to

$$p(x,y,z,t) = \int_{-\infty}^{\infty} F(k_x^*,k_y^*,\tilde{S})\left(\frac{2\pi}{z}\right)\left[\det\left|\frac{\partial^2 W}{\partial k_x \partial k_y}\right| \right]^{-1/2}_{k_x^*,k_y^*} \tag{3.23}$$

$$e^{ik_x^* x + ik_y^* y - izW(k_x^*,k_y^*,k) - i\frac{\pi}{2}\,\mathrm{sgn}W''}\, dS$$

Using k_x^* and k_y^* from eqns. (3.21), we evaluate

$$\left[\det\left|\frac{\partial^2 W}{\partial k_x \partial k_y}\right|\right]^{-1/2}_{k_x^*,k_y^*} = \frac{k^2 - k_x^{*2} - k_y^{*2}}{k} = k\,\frac{z^2}{r^2}$$

and $$\tilde{S} = S - k_y^* = S\left(1 - M\,\frac{y}{r}\right)$$

where the relation $k = MS$ has been used.

These expressions are substituted into eqn. (3.23) to give, after some algebra

$$p(x,y,z,t) = \frac{1}{2\pi b_o}\int_{-\infty}^{\infty} iL_o\{S(1-M\tfrac{y}{r})\}\,\frac{\sin\{s_o\tilde{S}[\tan\Lambda\,(1-M\frac{y}{r}) - M\frac{x}{r}]\}}{S[\tan\Lambda\,(1-M\frac{y}{r}) - M\frac{x}{r}]} \tag{3.24}$$

$$\frac{z}{r^2}MS\; e^{iS(Mr-t)}\; dS$$

where we have substituted $U_c = 1/\tan\Lambda$.

Equation (3.24) could equivalently have been expressed as an integral over aerodynamic frequency $\tilde{S}$ rather than observed frequency S. The latter seems the more reasonable choice because it clearly indicates that we are evaluating the pressure as an inverse transform of the farfield frequency spectrum.

$$p(x,y,z,t) = \frac{1}{2\pi}\int_{-\infty}^{\infty} P(S)\; e^{-iSt}\; dS$$

We change to spherical coordinates, with reference to fig. 4.

$$x = r\cos\theta\sin\psi$$

$$y = r\cos\theta\cos\psi$$

$$z = r\sin\theta$$

$\tilde{S}$ and S are now related by

$$\tilde{S} = S(1-M\cos\theta\cos\psi) \tag{3.25}$$

and equation (3.24) becomes

$$p(r,\theta,\psi,t) = \frac{1}{2\pi r}\int_{-\infty}^{\infty} i\,\frac{1}{b_o}\,L_o\{S(1-M\cos\theta\cos\psi)\} \frac{\sin\{s_o S[\tan\Lambda(1-M\cos\theta\cos\psi)-M\cos\theta\sin\psi]\}\,\sin\theta}{S[\tan\Lambda(1-M\cos\theta\cos\psi)\ -M\cos\theta\sin\psi]} MSe^{iS(Mr-t)}dS \tag{3.26}$$

3.4 Directivity of Blade/Vortex Interaction Noise

Using relation (3.25), we define the acoustic directivity factor appearing in eqn. (3.26) as

$$D(\theta,\psi,\tilde{S}) = \frac{\sin\{s_o\tilde{S}[\tan\Lambda-M\cos\theta\sin\psi/(1-M\cos\theta\cos\psi)]\}\sin\theta}{(1-M\cos\theta\cos\psi)^2\{s_o\tilde{S}[\tan\Lambda-M\cos\theta\sin\psi/(1-M\cos\theta\cos\psi)]} \tag{3.27}$$

Eqn. (3.27) is expressed as a function of aerodynamic frequency $\tilde{S}$, in conformity with the conventional interpretation of the directivity factor as a representation of the acoustic field due to a source of prescribed frequency. For a given value of $\tilde{S}$, observed frequency S varies throughout the field, so that writing the directivity in terms of S would have been misleading.

Using eqn. (3.27), the farfield pressure of eqn. (3.26) is written

$$p(r,\theta,\psi,t) = (1-M\cos\theta\cos\psi)^2\frac{Ms_o}{2\pi r}\int_{-\infty}^{\infty} iL_o\{S(1-M\cos\theta\cos\psi)\}D\{\theta,\psi,S(1-M\cos\theta\cos\psi)\}$$

$$Se^{iS(Mr/b_o-t)}\,dS \qquad (3.28)$$

or equivalently, in terms of $\tilde{S}$,

$$p(r,\theta,\psi,t) = \frac{Ms_o}{2\pi r}\int_{-\infty}^{\infty} iL_o\{\tilde{S}\}D\{\theta,\psi,\tilde{S}\}\tilde{S}\, e^{i[\tilde{S}/(1-M\cos\theta\cos\psi)](Mr/b_o-t)}\,d\tilde{S} \qquad (3.29)$$

where r has been redefined in dimensional terms.

The directivity factor of eqn. (3.27) can be expressed in terms of $\tilde{k}$, the acoustic wavenumber at the blade location.

Using the relation $\tilde{k} = M\tilde{S}$, we write

$$D(\theta,\psi,\tilde{k}) = \frac{\sin\{s_o\tilde{k}[\tan\Lambda/_M - \cos\theta\sin\psi/_{(1-M\cos\theta\cos\psi)}]\}\sin\theta}{(1-M\cos\theta\cos\psi)^2\{s_o\tilde{k}[\tan\Lambda/_M - \cos\theta\sin\psi/_{(1-M\cos\theta\cos\psi)}]\}} \qquad (3.30)$$

For the case of the source dimension much smaller than a wavelength ($\tilde{k}s_o \ll 1$), eqn. (3.30) is seen to reduce to the directivity factor associated with a convected point dipole, derived in appendix A as

$$D(\theta,\psi) = \frac{\sin\theta}{(1-M\cos\theta\cos\psi)^2} \tag{3.31}$$

This expression applies in cases where the important blade/vortex interaction is confined to the tip region, as in the single rotor flow geometry sketched in fig. 1.

For effective blade/vortex interaction lengths of the order of the blade length ($\tilde{k}s_0 >> 1$), more likely to occur for tandem rotor blade/vortex interactions, the directivity pattern becomes highly concentrated about the combination for which

$$\frac{\tan\Lambda}{M} - \frac{\cos\theta\sin\psi_{crit}}{1-M\cos\theta\cos\psi_{crit}} = 0 \tag{3.32}$$

For these critical values of θ and ψ, the directivity factor is also given by the point dipole expression, eqn. (3.31). $D(\theta,\psi_{crit})$ is plotted in fig. 5 for M = .53 at various values of Λ. (This corresponds to the numerical case investigated in Section 6.) The maximum value of ψ_{crit} barely exceeds 50° for these cases, indicating that the acoustic power is beamed strongly forward.

3.5 The Acoustic Signal Due to a Repeated Transient

The acoustic pressure of eqn. (3.28) is that due to a single blade/vortex interaction. For helicopter application, this transient is repeated at the blade passage frequency $\Omega = m\alpha$, where α is the angular velocity of the rotor and m the number of blades. (We note that although the frequency content of the transient is Doppler shifted due to motion of the blades, the repetition of the signal is perceived at the blade

passage frequency for the case of a hovering helicopter.)

For notational convenience, we write eqn. (3.28) as

$$p(t) = \int_{-\infty}^{\infty} P(S)e^{-iSt}\,dS$$

so that

$$P(S) = \frac{1}{2\pi}\int_{-\infty}^{\infty} p(t)e^{iSt}\,dt.$$

The repeated signal is given by

$$p_r(t) = \sum_{n=-\infty}^{\infty} p(t-nT) \tag{3.33}$$

where T is the (nondimensional) period,

$$T = \frac{2\pi}{\Omega}\,\frac{U}{b_o} \tag{3.34}$$

The spectrum of the repeated signal is

$$P_r(S) = \frac{1}{2\pi}\int_{-\infty}^{\infty} \sum_{n=-\infty}^{\infty} p(t-nT)e^{iSt}dt = \sum_{n=-\infty}^{\infty} e^{iSnT}P(S) \tag{3.35}$$

We can write

$$\sum_{n=-\infty}^{\infty} e^{iSnT} = 2\pi \sum_{m=-\infty}^{\infty} \delta(ST-2\pi m)$$

$$= \frac{2\pi}{T} \sum_{m=-\infty}^{\infty} \delta(S-\frac{2\pi m}{T}) = \frac{\Omega b_o}{U} \sum_{m=-\infty}^{\infty} \delta(S-m\frac{\Omega b_o}{U}) \tag{3.36}$$

so that

$$P_r(S) = \frac{\Omega b_o}{U} \sum_{m=-\infty}^{\infty} \delta(S-m\frac{\Omega b_o}{U})\ P(S) \tag{3.37}$$

and

$$P_r(t) = \frac{\Omega b_o}{U} \sum_{m=-\infty}^{\infty} P(m\frac{\Omega b_o}{U})\ e^{-im\frac{\Omega b_o}{U}t} \tag{3.38}$$

Denoting $S_m = m\frac{\Omega b_o}{U}$, the repeated acoustic signal is then written as the Fourier series

$$p_r(r,\theta,\psi,t) = i(1-M\cos\theta\cos\psi)^2 \frac{Ms_o}{2\pi r} \tag{3.39}$$

$$\times \frac{\Omega b_o}{U} \sum_{m=-\infty}^{\infty} L_o\{S_m(1-M\cos\theta\cos\psi)\}D\{\theta,\psi,S_m(1-M\cos\theta\cos\psi)\}S_m e^{iS_m(Mr/b_o-t)}$$

4. THE BETZ VORTEX MODEL

The Betz [6] vortex model predicts the approximate structure of a fully rolled up lift generated trailing vortex given the spanwise lift distribution on a flat wing. It does not treat the intermediate stages between the initially flat trailing vortex sheet and the rolled up vortex. The rollup process is assumed to be inviscid and two dimensional.

We use the Betz method to predict the velocity profile in the tip vortex corresponding to an assumed form for the steady spanwise blade loading distribution. Donaldson's results suggest that only the vorticity situated between the helicopter blade tip and the position of maximum spanwise loading rolls up into the tip vortex. We assume that the maximum loading occurs at 75% of blade span, [7] and that the loading falls off monotonically to zero at the blade tip, so that only the outer 25% of blade radius contributes to tip vortex structure. The tangential blade velocity is taken to be uniform over this length.

With reference to fig. 6, the spanwise coordinate on the blade is y, with y=0 at 75% span, and y=L at the blade tip. The radial coordinate in the fully rolled up trailing vortex is r. We denote the spanwise distribution of bound circulation as $\Gamma_b(y)$, and the radial distribution of circulation in the vortex as $\Gamma_v(r)$.

The result of the Betz method is the determination of a function r=r(y) such that $\Gamma_b(y) = \Gamma_v(r)$ at corresponding values of r and y, subject to the constraint that Γ_b and Γ_v be related by three conservation relations for two dimensional systems:

I. The circulation is conserved.

$$\Gamma_b(0) = \Gamma_o = -\int_o^L \frac{d\Gamma_b(y)}{dy}\, dy = \int_o^{r_{max}} \frac{d\Gamma_v}{dr}\, dr \tag{4.1}$$

II. The centroid of vorticity remains at a fixed spanwise location.

$$\bar{y}(0) = \frac{1}{\Gamma_o}\int_L^o y\, \frac{d\Gamma_b(y)}{dy}\, dy \tag{4.2}$$

III. The second moment of vorticity is conserved, $J_v=J_b=J$.

$$J = \int_L^o [\bar{y}(0)-y]^2\, \frac{d\Gamma_b(y)}{dy}\, dy = \int_o^{r_{max}} r^2\, \frac{d\Gamma_v(r)}{dr}\, dr \tag{4.3}$$

where r_{max} is the radius within which all the vorticity is contained in the fully developed vortex.

Equations (4.1,2,3) are further assumed to apply piecewise, beginning at the wing tip, to successive portions of the sheet in toward the wing root:

$$\int_L^{y_1} \frac{d\Gamma_b(y)}{dy}\, dy = \int_o^{r_1} \frac{d\Gamma_v(r)}{dr}\, dr \tag{4.4}$$

$$\bar{y}(y_1) = \frac{1}{\Gamma_b(y_1)}\int_L^{y_1} y\, \frac{d\Gamma_b(y)}{dy}\, dy \tag{4.5}$$

$$\int_{L}^{y_1} [\overline{y}(y_1) - y]^2 \frac{d\Gamma_b(y)}{dy}\, dy = \int_{o}^{r_1} r^2 \frac{d\Gamma_v(r)}{dr}\, dr \qquad (4.6)$$

Rossow [12] uses the above equations to obtain the relation between r and y as

$$r = \left| \frac{1}{\Gamma_b(y)} \int_{L}^{y} \Gamma_b(y_1) dy_1 \right| \qquad (4.7)$$

The circumferential velocity in an axially symmetric vortex is found from

$$v_\theta = \frac{\Gamma_v(r)}{2\pi r} = \frac{\Gamma_b\{y(r)\}}{2\pi r} \qquad (4.8)$$

5. APPLICATION TO A NUMERICAL SCHEME

In this section we outline the adaptation of previously derived results to numerical computation.

5.1 The Betz Model

Using eqns. (4.7) and (4.8) it is quite straightforward to develop a numerical procedure to predict the structure of the trailing vortex, given an assumed form for the spanwise distribution of bound circulation on the blade $\Gamma_b(y)$.

Referring to section 4, eqn. (4.7) is integrated numerically from $y = 0$ (corresponding to $r = 0$ in the rolled up vortex) to $y = L$ (corresponding to r_{max}). For each pair of values (r, y) thus found, eqn. (4.8) is used to evaluate the circumferential velocity $v_\theta(r)$. The vortex is assumed to be irrotational for $r > r_{max}$, so that we use a potential vortex model ($v_\theta \sim 1/r$) for this region.

We note that $v_\theta = 0$ is always used at $r = 0$. (This is necessary for subsequent computation.)

5.2 Blade/Vortex Interactions

From the circumferential velocity distribution computed as in section 5.1 and blade/vortex separation h, we begin by computing the upwash in the plane of the airfoil ($w_o(\xi)$ of eqns (2.1). The Fourier transform indicated in eqns. (2.1) is then computed numerically, using a fast Fourier transform (FFT) subroutine. The application of the FFT subroutine is described in reference [13].

Given blade/vortex interaction angle Λ, the upwash spectrum at the airfoil location $W(\tilde{S})$ is obtained from eqn. (2.8), and used in eqn. (2.11) to give the spectrum of the unsteady lift $L_o(\tilde{S})$. The inverse transform indi-

cated in eqn. (2.12) is then evaluated through the use of the FFT subroutine to give the unsteady lift due to a single blade/vortex interaction, $L(t')$.

Similarly for the pressure, the inverse transform of the farfield spectrum is evaluated using the FFT subroutine to give the farfield signal (due to one blade/vortex interaction) of eqn. (3.28). Strictly speaking, we should evaluate the Fourier series of eqn. (3.29) to give the signal due to a series of transients repeated at the blade passage frequency Ω. However, numerical evaluation of eqn. (3.28) shows that the nonzero extent of the transient due to a single interaction is of much shorted duration than the blade passage period T, so that the transient decays too rapidly to contribute acoustic energy to any subsequent pulses. Therefore, an interval of the transient signal of duration T looks identical to one period of the signal due to repeated interactions.

6. RESULTS AND DISCUSSION

The model is applied to three tip loading configurations. For the vortex corresponding to each of these cases, numerical results are presented for the unsteady lift experienced by a blade interacting with the vortex and the associated acoustic signal over a range of interaction geometries. General features of the noise due to blade/vortex interaction are considered, and results of some recent experimental attempts to minimize the problem through alteration of tip vortex structure are discussed in light of the theory.

6.1 Cases Investigated

Inputs to the model are:

(1) b_o, blade semichord

(2) U_{eff}, effective blade velocity

(3) $\Gamma_b(y)$, distribution of bound circulation on the blade tip shedding the vortex for input to the Betz model

(4) h, blade/vortex separation

(5) Λ, blade/vortex angle

(6) s_o, effective blade/vortex interaction length

(7) r,θ,ψ, coordinates of the observer, fig. 4

(8) Ω, blade passage frequency

(9) ρ,c, fluid density and sound speed, taken for air at STP

Helicopter parameters used to perform the computations were those of a Bell model UH-1H. Relevant specifications are listed below (from ref. [14]).

Number of Blades	2
Rotor Diameter	48 ft.
Blade Semichord	10.5 in.
avg. tip speed	780 ft/sec
avg. gross weight	8000 lbs.
blade passage frequency	65 rad/sec

To obtain an order of magnitude estimate of the maximum section load, maximum loading was assumed at 75% blade radius, with spanwise loading taken to fall off linearly from a maximum (L_{max}) to zero at the blade root and tip. For two 24 ft blades supporting an 8000 lb helicopter, this gives L_{max} = 333 lbs/ft. Denoting maximum circulation by Γ_o, the relation $L_{max} = \rho U \Gamma_o$ from lifting line theory (with U at 75% radius) gives Γ_o = 238 ft^2/sec.

The three spanwise distributions of bound circulation assumed for the blade tip (outboard 25% span) are presented in fig. 7. Γ_o is the same for the three cases (elliptical, linear, and cos^2 circulation distributions).

For the acoustic parameters, effective blade/vortex interaction length s_o was estimated as 2/3 of the blade length, or s_o = 16 ft. Effective blade velocity was taken to be $.75U_{tip}$, or U_{eff} = 585 ft/sec, corresponding to a Mach number of .53. Calculations were performed for blade/vortex angle Λ = 0, 15, and 30°, with blade/vortex separation distance h = 0, .2, .5, 1, and 2 blade semichords investigated for each value of Λ.

Observer coordinates were selected to yield the most intense acoustic signal for each case. (θ, ψ_{crit} corresponding to D_{max} from eqns. (3.31) and (3.32) were computed for each value of Λ.) r = 1000 ft was used.

The cases investigated are summarized below.

I. Tip Load Distribution (Γ_0 = 238 ft^2/sec, y = 0 at 75% span, y = L at blade tip)

i) elliptical $\Gamma = \Gamma_0 \sqrt{1 - (y/L)^2}$

ii) Linear $\Gamma = \Gamma_0(1 - y/L)$

iii) $\cos^2$ $\Gamma = \Gamma_0 \cos^2(\frac{\pi y}{2L})$

II. Blade/Vortex Interaction and Acoustic Parameters

s_0 = 16 ft

U_{eff} = 585 ft/sec (M = .53)

r = 1000 ft

$\Lambda = 0°$, $\theta = 40.7°$, $\psi = 0°$

$\Lambda = 15°$, $\theta = 38.0°$, $\psi = 23.3°$

$\Lambda = 30°$, $\theta = 18°$, $\psi = 52.7°$

6.2 Results

Results are presented in figs. 8 through 27.

fig. 8 - circumferential velocity profile in the vortices corresponding to each loading case

fig. 9 - 17 - unsteady section lift experienced at a spanwise station during blade/vortex interaction

fig. 18 - 26 - farfield acoustic signal due to blade/vortex interaction

fig. 27 - comparison of acoustic intensities

6.3 Discussion

i) Trailing Vortex (fig. 8)

The structure of the trailing vortex, as predicted by the Betz theory, is profoundly influenced by the slope of the loading function at the blade tip. In the case of the elliptical load distribution, for which the loading falls off with infinite slope at the blade tip, a square-root singularity in circumferential velocity is predicted at r = 0. For the $\cos^2$ load distribution, zero slope at the blade tip leads to $v_\theta = 0$ and $\frac{dv}{dr} = 0$ at r = 0, and the maximum circumferential velocity occurs at a finite distance from the vortex center. The linear load distribution has a finite nonzero slope at the blade tip, giving a finite nonzero velocity at r = 0 (requiring a velocity discontinuity here).

Adaptation of the theory to numerical computation requires $v_\theta = 0$ at r = 0. This acts to reduce the severity of the singularity and the discontinuity encountered in the elliptical and linear loading cases. The effect of viscosity in the real fluid would also moderate these abrupt features of the velocity profile. (Viscous effects were not considered here to avoid unnecessary complication of the analysis.)

ii) Upwash

The distribution of circumferential velocity in the trailing vortex represents the upwash encountered by a blade at zero blade/vortex separation. With an increase in separation, we see two effects:

(1) The amplitude of the upwash signal is decreased, as circumferential velocity falls off with an increase in distance from the vortex center (except in the immediate vicinity of r = 0 for the $\cos^2$ loading case).

(2) The high frequency content of the upwash transient is diminished; the signal is smoothed out as the blade passes further outside abrupt fluctuations in circumferential velocity that are concentrated about the center of the vortex.

The blade experiences the most concentrated, sharply peaked upwash signal (i.e. largest high frequency content) through interaction with the trailing vortex for the case of elliptical loading. A more gradual variation in upwash is experienced for the cases of the linear and $\cos^2$ loading distributions. The peak to peak amplitude of the upwash signal is largest for elliptical loading, less for the $\cos^2$ case, and smallest for the case of linear loading. With an increase in sweep angle (Λ), the upwash signal becomes less concentrated, i.e. the high frequency content of the signal is diminished.

iii) Unsteady lift (figs. 9 - 17)

The character of the unsteady lift signal can be expected to resemble that of the upwash signal. Accordingly, the peak to peak amplitude of the unsteady lift signal is largest for the case of elliptical loading, less for the $\cos^2$ case, and smallest for linear loading, corresponding to the relative amplitudes of the upwash signals. An increase in sweep angle spreads out the unsteady lift signal as it does the upwash.

The relationship between unsteady lift and upwash is governed by the Filotas "lift transfer function", which gives a decrease in the amplitude of the unsteady lift signal with an increase in gust frequency and/or sweep angle. We note also that the transfer function is unity for a zero frequency gust (steady upwash case), but introduces an aerodynamic phase shift between upwash and unsteady lift at higher gust frequencies.

Consequently, the degree of harmonic distortion in the unsteady lift signal (relative to the upwash signal) is seen to increase with an increase in the high frequency content of the upwash signal. This is particularly evident for the case of elliptical loading at small values of h, as this upwash signal is the richest in high frequency content.

iv) Acoustic Signal (figs. 18 - 26)

We have modelled the helicopter blade as a finite line of acoustic dipoles. It is not surprising, then, that analysis of the acoustic radiation from a single convected point dipole affords much insight into the problem.

The farfield sound due to a convected point dipole of amplitude F_o (point force) and sinusoidal frequency ω_o is derived in appendix A as

$$p(r,\theta,\psi,t) = \frac{F_o}{2\pi r}\,\omega_o\,\frac{1}{c}\,D(\theta,\psi)\,e^{-i\left(\frac{\omega_o}{1-M\cos\theta\cos\psi}\right)(t-r/c)}$$

where the directivity factor $D(\theta,\psi) = \dfrac{\sin\theta}{(1-M\cos\theta\cos\psi)^2}$

Two features of the dipole expression are of interest here:

(a) The magnitude of the acoustic pressure is proportional to frequency, ω_o.

(b) As indicated in section 3.4, convection acts to concentrate the acoustic power in the forward direction, giving rise to an increase in the value of the maximum acoustic pressure attained (over that of the nonconvected case).

(a) Frequency Dependence

The results clearly indicate the dependence of the peak acoustic pressure on frequency. We find, for example, that at h = 0 the amplitude of the upwash signal associated with elliptical loading is about twice that for the $\cos^2$ case, but that the acoustic signal for $\cos^2$ loading is 34 db down. This dramatic difference (corresponding to a fifty fold decrease in acoustic pressure) can be attributed to the abrupt (high frequency) character of the unsteady lift signal of the elliptical case relative to the gradual (low frequency) character of the $\cos^2$ case. Similarly, for small values of h, $\cos^2$ loading gives a signal that is 10 db down from the corresponding linear loading case, even though the amplitude of the unsteady lift signal for the $\cos^2$ case is larger.

(b) Effect of Sweep

The introduction of sweep causes a substantial reduction in radiated noise, as demonstrated in fig. 27. As already indicated, an increase in Λ diminishes the high frequency content of the unsteady lift signal, which can be taken as a partial explanation for the change.

A more subtle effect is the relationship between Λ and the convection speed of the lift pattern through the fluid. Since the convected Mach number of the wave along the moving blade is $M/\tan\Lambda$, the effective Mach number of the wave through the still fluid is

$$M_{eff} = \sqrt{M^2 + \left(\frac{M}{\tan\Lambda}\right)^2} = M/\sin\Lambda \qquad (6.1)$$

so that $M = \sin\Lambda$ is the boundary between supersonic and subsonic wave speeds.

Disturbances moving at subsonic speeds with respect to the still fluid radiate no sound; for $M < \sin\Lambda$ the only sound that is generated originates at the ends of the blades and is due to the finite dimensions of the source. For this case values of (θ, ψ_{crit}) satisfying eqn. (3.32) do not exist, so that no concentration of the acoustic signal occurs. As a result, the radiated noise is greatly reduced. (This case was not investigated numerically.)

Conversely, disturbances moving at supersonic speeds are efficient acoustic radiators, and the intensity of the peak acoustic signal increases with Mach number. With reference to fig. 27, the diminution of the peak signal for $\Lambda = 30°$ is due, in part, to the fact that the disturbance velocity is barely supersonic for this case ($M_{eff} = 1.06$).

At large values of Λ it must be remembered that the two dimensional aerodynamic model used is no longer valid, due to three dimensional effects at the blade tip. At some point, the tip/vortex interaction becomes the predominant acoustic source.

6. Blade-slap Minimization Through Tip Modification

Potential methods of blade slap minimization include reduced tip speed, reduced disc loading, changes in blade design (area, twist, and shape) and alteration of blade tip shape.[1] Of these, alteration of tip shape is of particular relevance to the present study, as this technique entails changes in tip vortex structure that minimize noise.

The most significant result of this investigation with regard to tip design is that the slope of the spanwise loading distribution at the blade tip strongly influences tip vortex structure and the associated intensity of noise due to blade/vortex interaction. This result is consistent with recent

experimental findings [8] that show substantial reduction in blade slap intensity through the use of a tapered ("ogee") blade tip. (fig. 28a)

Another technique that has yielded positive results [2] makes use of a "sub-wing" tip (fig. 28b). This design apparently divides the tip vortex into two less intense twin vortices that destructively interact to produce a diffuse trailing vortex. However, more quantitative acoustic data is needed to judge the efficacy of this method.

7. CONCLUSIONS

Blade/vortex interaction is an important source of helicopter blade slap. Several experimental studies indicate effective blade slap minimization through modification of tip design in an effort to alter vortex structure.

Theoretical analysis of blade/vortex interaction, through application of linear unsteady aerodynamics and the acoustics of a moving source, is able to account for the essential role played by many of the parameters that govern the occurrence of blade slap.

The numerical model developed to extend the analysis to tip vortices of arbitrary structure constitutes a powerful investigative tool. The method affords useful insight into the relationship between the character of the tip vortex and the associated noise due to blade/vortex interaction. The intensity of the noise was found to be quite sensitive to changes in tip vortex structure.

This model is applicable to blade/vortex interactions at small oblique angles, for which the interaction occurs over a large portion of the blade span. Such interactions are probable for tandem rotor helicopters. For single rotors, blade/vortex interactions are likely to occur at large angles, for which the interaction is confined to the blade tip region. Additional theoretical modeling is required to account for the three dimensional aerodynamic effects associated with this case.

Other effects the model is not equipped to handle include blade or self-induced motion of the vortex filaments during blade/vortex interaction, curvature of the vortex filaments, and blade rotation. These problems deserve future study.

The aerodynamic theory used to model blade/vortex interaction strictly applies only to the case of a low frequency gust in an incompressible fluid. Making the appropriate low frequency assumption that the blade chord is smaller than a wavelength, we neglect chordwise pressure variation in the unsteady lift calculation and model the blade as a line of dipoles in the analysis of the acoustic field. At higher gust frequencies or higher Mach numbers, compressibility effects become important, and a more powerful aerodynamic theory such as that due to Amiet [15] is required. The simpler aerodynamic model used here is sufficient to account for the essential details of the relationship between vortex structure and the acoustic pulse. The additional refinement obtainable from consideration of compressibility and high frequency effects was felt to be unnecessary for this initial study. The extension to include the full effects of compressibility is currently underway.

APPENDIX A: Sound Field Due to a Convected Point Dipole

The calculation of the sound field due to a convected point dipole follows the analysis of section 3 (for a moving line of phased dipoles). The simpler boundary condition, however, gives the farfield pressure signal in integrable form for the case of harmonic oscillation.

We consider a point force of magnitude f(t), oriented normal to the x-y plane, moving with velocity U in the y direction.

The governing equation for the unsteady pressure is

$$\nabla^2 p = \frac{1}{c^2} \frac{\partial^2 p}{\partial t^2} \tag{A1}$$

with boundary conditions

$$\Delta p = p(x,y,0^-) - p(x,y,0^+) = \delta(x)\delta(y-Ut)f(t) \tag{A2}$$

We introduce the Fourier transform in x,y, and t, defining the transform pair

$$\begin{aligned} p(x,y,z,t) &= \frac{1}{(2\pi)^3} \iiint_{-\infty}^{\infty} P(k_x,k_y,\omega;z) e^{i(k_x x + k_y y - \omega t)} dk_x dk_y d\omega \\ P(k_x,k_y,\omega;z) &= \iiint_{-\infty}^{\infty} p(x,y,z,t) e^{-i(k_x x + k_y y - \omega t)} dx dy dt \end{aligned} \tag{A3}$$

The Fourier transform of the boundary condition is given by

$$\Delta P(k_x,k_y,\omega) = \iiint_{-\infty}^{\infty} \delta(x)\delta(y-Ut)f(t) e^{-i(k_x x + k_y y - \omega t)} dx dy dt \tag{A4}$$

From the properties of the delta function, the only contribution to the y integral occurs at y = Ut, giving

$$\Delta P(k_x,k_y,\omega) = \int\int\int\int_{-\infty}^{\infty} f(t)\delta(x)e^{-ik_x x+i(\omega-k_y U)t}\,dxdt \qquad (A5)$$

We define the frequency $\tilde{\omega} = \omega-k_y U$, recognizing that a frequency $\tilde{\omega}$ located on the moving boundary is perceived at Doppler shifted frequency ω in the field. Eqn. (A5) is then written

$$\Delta P(k_x,k_y,\omega) = \int_{-\infty}^{\infty}\delta(x)e^{-ik_x x}\left\{\int_{-\infty}^{\infty} f(t)e^{i\tilde{\omega}t}\,dt\right\}dx \qquad (A6)$$

Defining the transform pair

$$\begin{aligned} f(t) &= \int_{-\infty}^{\infty} F(\tilde{\omega})e^{-i\tilde{\omega}t}\,d\tilde{\omega} \\ F(\tilde{\omega}) &= \frac{1}{2\pi}\int_{-\infty}^{\infty} f(t)e^{i\tilde{\omega}t}\,dt \end{aligned} \qquad (A7)$$

we identify the bracketed term in eqn. (A6) to be $2\pi F(\tilde{\omega})$.

Then

$$\Delta P(k_x,k_y,\omega) = 2\pi F(\tilde{\omega})\int_{-\infty}^{\infty}\delta(x)e^{-ik_x x}\,dx \qquad (A8)$$

Contribution to the x integral occurs at x = 0, giving the Fourier transform of the boundary condition as

$$\Delta P(k_x,k_y,\omega) = 2\pi F(\tilde{\omega}) \tag{A9}$$

where $\tilde{\omega} = \omega - k_y U$

Taking the Fourier transform of eqn. (A1) leads, as in section 3, to the expression

$$p^{\pm}(x,y,z,t) = A^{\pm}(k_x,k_y,\omega)e^{\pm iz\sqrt{k^2-k_x^2-k_y^2}} \tag{A10}$$

Applying the boundary condition of eqn. (A9) and imposing the additional requirement

$$\frac{\partial p^+}{\partial z} = \frac{\partial p^-}{\partial z}\bigg|_{z=0} \tag{A11}$$

gives the constants $A^{\pm} = \mp \pi F(\tilde{\omega})$.

The unsteady pressure is then given by the Fourier integral indicated in eqn. (A3),

$$p(x,y,z,t) = -\frac{1}{8\pi^2}\int_{-\infty}^{\infty}\iiint F(\tilde{\omega})e^{i(k_x x+k_y y-\omega t)+iz\sqrt{k^2-k_x^2-k_y^2}}\,dk_x,dk_y d\omega \tag{A12}$$

As in section 3, the k_x and k_y integrations in the asymptotic farfield limit can be evaluated by the method of stationary phase, giving the farfield acoustic pressure as

$$p(x,y,z,t) = \frac{1}{4\pi}\int_{-\infty}^{\infty} iF(\tilde{\omega})\,\frac{z}{r^2}\,\frac{\omega}{c}\,e^{-i\omega(t-r/c)}\,d\omega \qquad (A13)$$

Changing to polar coordinates, with reference to fig. 4 ,

$x = r\cos\theta\sin\psi$

$y = r\cos\theta\cos\psi$

$z = r\sin\theta$

gives

$$p(r,\theta,\psi,t) = \frac{1}{4\pi r}\int_{-\infty}^{\infty} iF(\tilde{\omega})\sin\theta\,\frac{\omega}{c}\,e^{-i\omega(t-r/c)}\,d\omega \qquad (A14)$$

where $\tilde{\omega} = \omega(1-M\cos\theta\cos\psi)$

For the case of a simple harmonic dipole of frequency ω_0,

$$f(t) = F_0 e^{-i\omega_0 t} \qquad (A15)$$

the transform is given by

$$F(\tilde{\omega}) = \frac{1}{2\pi}\int_{-\infty}^{\infty} f(t)e^{i\tilde{\omega}t}dt = \frac{F_0}{2\pi}\int_{-\infty}^{\infty} e^{i(\tilde{\omega}-\omega_0)t}dt$$

$$= F_0\delta(\tilde{\omega}-\omega_0) \qquad (A16)$$

Using $\omega = \tilde{\omega}/(1-M\cos\theta\cos\psi)$, eqn. (A14) then becomes

$$p(r,\theta,\psi,t) = \frac{F_0}{2\pi r}\int_{-\infty}^{\infty} \delta(\tilde{\omega}-\omega_0)\frac{\sin\theta}{(1-M\cos\theta\cos\psi)^2}\,\frac{\tilde{\omega}}{c}\,e^{-i\left(\frac{\tilde{\omega}}{1-M\cos\theta\cos\psi}\right)(t-r/c)}\,d\tilde{\omega} \qquad (A17)$$

Contribution to the integral occurs at $\tilde{\omega} = \omega_o$, giving the unsteady pressure as

$$p(r,\theta,\psi,t) = \frac{F_o}{2\pi r} \frac{\omega_o}{c} D(\theta,\psi) e^{-i\left(\frac{\omega_o}{1-M\cos\theta\cos\psi}\right)(t-r/c)} \tag{A18}$$

where the directivity factor is defined by

$$D(\theta,\psi) = \frac{\sin\theta}{(1-M\cos\theta\cos\psi)^2} \quad . \tag{A19}$$

APPENDIX B: Lift Transfer Function of Filotas Theory

The lift transfer function is used to calculate the unsteady lift due to an oblique sinusoidal gust impinging on a two dimensional airfoil in incompressible flow (fig. B1). For a gust of nondimensional wavenumber $\sigma = \sigma_o b_o$,

$$T(\sigma,\Lambda) = \frac{\exp\{-i\sigma[\cos\Lambda - \frac{\pi(\frac{\pi}{2}-\Lambda)(1+\frac{1}{2}\sin\Lambda)}{1+2\pi\sigma(1+\frac{1}{2}\sin\Lambda)}]\}}{\sqrt{1+\pi\sigma(1+\cos^2\Lambda+\pi\sigma\sin\Lambda)}}$$

APPENDIX C: Computer Program

```
      COMPLEX*8 C(2048),W(2048),CL,T,W0,L0,P
      COMPLEX*8 CMPLX,CEXP
      REAL L,LAMBDA,MACH,VTHET(1024),VR(1024)
      DIMENSION GRAF1(512,7)
      DIMENSION UU(514),V1(514),V2(514),V3(514),V4(514),V5(514),V6(514)
      COMMON W,C,VR,R,THETA,PSI,LAMBDA,OMEGA,GAMMA,GAMMA0,MACH,RHO,S0,
     &       B0,U,H,PI,UFLO,
     &       COSLAM,TANLAM,COTHET,COSPSI,
     &       DS,DSBAR,DT,DTP,DELZ,DR,
     &       N,N2,N4
C     VARIABLES USED IN MAIN PROGRAM:
C     BLDS: NO. OF ROTOR BLADES
C     B0:BLADE SEMICHORD(FEET)
C     CL:UNSTEADY SECTION LIFT COEFFICIENT FROM FILOTAS THEORY
C     DIREC:DIRECTIVITY FACTOR,EQN. 3.27
C     GAMMA0:CIRCULATION(FT**2/SEC)
C     GAMMA:NONDIMENSIONAL CIRCULATION(GAMMA=GAMMA0/B0*U)
C     GC:GRAVITATIONAL CONSTANT(LBM*FT/LBF*SEC**2)
C     H:VORTEX TO BLADE DISTANCE IN SEMICHORDS, SEE FIG 3
C     LAMBDA:ANGLE BETWEEN BLADE AND VORTEX, FIG.3 (RAD)
C     MACH:BLADE MACH NUMBER
C     OMEGA:ANGULAR FREQUENCY OF ROTOR(RAD/SEC)
C       (CORRESPONDS TO ALPHA OF TEXT)
      P:PRESSURE(LBF/FT**2)
C     R,THETA,PSI:COORDINATE SYSTEM OF FIG.3
C     S0:BLADE INTERACTION LENGTH IN SEMICHORDS
C     U:BLADE VELOCITY(FT/SEC)
C     RHO:FLUID DENSITY(LBM/FT**3)
C     SBAR: STROUHAL FREQUENCY (AERODYNAMIC FREQUENCY)
C     S: DOPPLER SHIFTED STROUHAL FREQUENCY (ACOUSTIC FREQUENCY)
C     UFLO: USED IN UNDERFLOW CHECK
      PI=3.1415926
      B0=10.5/12.
      S0=16./B0
      R=1000.
      DEGRAD=2.0*PI/360.0
```

```
      LAMBDA=15.0*DEGRAD
      THETA=38.*DEGRAD
      PSI=23.3*DEGRAD
      U=585.
      MACH=U/1100.
      OMEGA=32.5
      GAMMA0=238.
      GAMMA=GAMMA0/(B0*U)
      GC=32.17
      RHO=.077/GC
      COTHET=COS(THETA)
      COSPSI=COS(PSI)
      COSLAM=COS(LAMBDA)
      TANLAM=TAN(LAMBDA)
      N=2048
      N2=N/2
      N4=N/4
      DO 100 M=1,N
      C(M)=CMPLX(0.0,0.0)
  100 CONTINUE
      TEN=10.0
      UFLO=TEN**(-40.0)
      Y0=0.0
C     H=0.0
C     ********************************************************************
C     * TO AVOID CONFUSION DUE TO THE NUMBER OF DIFFERENT CASES          *
C     * INVESTIGATED, SUBROUTINE CALLS AND PLOTTING ROUTINES HAVE NOT    *
C     * BEEN INCLUDED HERE. THE FOLLOWING SEQUENCE WOULD RETURN THE      *
C     * ACOUSTIC SIGNAL IN COMPLEX ARRAY C:                              *
C     *     CALL BETZ(NLOAD)  (SEE SUBROUTINE BETZ)                      *
C     *     CALL TRNSFM                                                  *
C     *     CALL SOUND                                                   *
C     SUBSTITUTION OF 'CALL LIFT' FOR 'CALL SOUND' WOULD RETURN THE    *
C     * UNSTEADY LIFT IN COMPLEX ARRAY C                                 *
C     ********************************************************************
```

```
      SUBROUTINE BETZ(NLOAD)
C     BETZ COMPUTES THE CIRCUMFERENTIAL VELOCITY DISTRIBUTION IN THE
C     TRAILING VORTEX USING THE BETZ ROLLUP MODEL OF CHAPTER 4, AND
C     EVALUATES THE VERTICAL VELOCITY W AS A FUNCTION OF Z, THE
C     SPATIAL COORDINATE PERPENDICULAR TO THE VORTEX.
C       (Z CORRESPONDS TO XCI IN TEXT, FIG 3)
C     SAMPLING INCREMENT IS DELZ, OVER INTERVAL VRTSEP
C     W(1) CORRESPONDS TO Z=0. W(1,...1024) CONTAIN VALUES FOR POSITIVE
C     Z, W(1025,...2048) VALUES FOR NEGATIVE Z. VALUES ARE STORED IN
C     ORDER OF INCREASING Z
C
C   COMPUTATION PROCEDURE:
C     EQN 4.7 IS INTEGRATED NUMERICALLY AND USED WITH EQN 4.8 TO COMPUTE
C     A SET OF N/2 CORRESPONDING VALUES RB(M) AND VCOR(M), THE RADIAL
C     COORDINATE AND CIRCUMFERENTIAL VELOCITY RESPECTIVELY IN THE
C     ROTATIONAL PORTION OF THE TAILING VORTEX. VCOR IS THEN SAMPLED
C     AT INCREMENT DR OVER N/2 POINTS TO COMPUTE VR, THE
O     CIRCUMFERENTIAL VELOCITY PROFILE IN THE TRAILING VORTEX. OUTSIDE
C     THE ROTATIONAL REGION (R>RB(N/2)) VR IS PROPORTIONAL TO 1/R.
C     UPWASH W IS COMPUTED FROM GEOMETRY.
C
C     NLOAD IS AN INDEX IDENTIFYING THE TIP LOADING CASE INVESTIGATED.
C     NLOAD=1 FOR ELLIPTICAL LOADING, 2 FOR LINEAR, AND 3 FOR COS**2.
      COMPLEX*8 C(2048),W(2048),CL,T,W0,L0,P
      COMPLEX*8 CMPLX,CEXP
      REAL L,LAMBDA,MACH,RB(1024),VCOR(1024),
     &VTHET(1024),VR(1024)
      INTEGER NLOAD
      COMMON W,C,VR,R,THETA,PSI,LAMBDA,OMEGA,GAMMA,GAMMA0,MACH,RHO,S0,
     &       B0,U,H,PI,UFLO,
     &       COSLAM,TANLAM,COTHET,COSPSI,
     &       DS,DSBAR,DT,DTP,DELZ,DR,
     &       N,N2,N4
      BLDS=2.
      VRTSEP=(2.0*PI/(BLDS*OMEGA*B0))*U*COSLAM
      VRTSEP=VRTSEP*4.
```

```
      DELZ=VRTSEP/FLOAT(N)
      DR=DELZ/1.95
      L=15./BO
      DY=(L/2.0)/N2
      SUM=0.0
      RB(1)=0.0
      VCOR(1)=0.0
C     YY IS THE SPANWISE COORDINATE. (CORRESPONDS TO Y OF TEXT) YY=0 AT
C     75% SPAN, YY=L/2 AT BLADE TIP. (IN TEXT, Y=L AT BLADE TIP)
C     VCOR(M) IS THE CIRCUMFERENTIAL VELOCITY CORRESPONDING TO
C     RADIUS RB(M) IN THE TRAILING VORTEX. (VTHETA, R USED IN TEXT)
      DO 100 M=2,N2
      FM=M-1
      YY=(L/2.0)-(FM*DY)
      GO TO  (14,15,16),NLOAD
   14 GG=(YY/(L/2.0))**2
      GAM=GAMMA*((1.0-GG)**0.5)
      GO TO 17
   15 GAM=GAMMA*(1.0-(YY*(2.0/L)))
      GO TO 17
   16 GG=(YY*PI)/(L/2.0)
      GAM=0.5*GAMMA*(1.0+COS(GG))
   17 CONTINUE
      SUM=SUM+(GAM*DY)
      RB(M)=ABS(SUM/GAM)
      VCOR(M)=GAM/(2.0*PI*RB(M))
  100 CONTINUE
C     CORAD IS THE RADIUS WITHIN WHICH ALL VORTICITY IS
C     CONTAINED. (RMAX OF TEXT)
      CORAD=RB(N2)
      VR(1)=0.0
      DO 400 M=2,N2
      FM=M-1
      RP=FM*DR
      IF (RP.GT.CORAD) GO TO 700
      DO 500 J=2,N2
```

```
      IF (RB(J).GT.RP) GO TO 600
      IF (J.EQ.N2) GO TO 600
  500 CONTINUE
  600 VR(M)=VCOR(J)
  400 CONTINUE
  700 CONTINUE
      DO 800 K=M,N2
      FK=K-1
      RP=FK*DR
      VR(K)=+GAMMA /(2.0*PI*RP)
  800 CONTINUE
      DO 250 I=1,N
      W(I)=CMPLX(0.0,0.0)
  250 CONTINUE
      DO 900 M=2,N2
      FM=M-1
      Z=FM*DELZ
      RZ=(Z**2+H**2)**0.5
      POS=RZ/DR
      K=IFIX(POS+0.5)
      IF (K.LT.2) K=2
      IF (K.GT.N/2) K=N/2
      ETA=ATAN2(H,Z)
C     VRTVEL IS VERTICAL VELOCITY
      VRTVEL=+VR(K)*COS(ETA)
      IF (K.EQ.N2) VRTVEL=+GAMMA /(2.0*PI*Z)
C     TAIL1 AND TAIL2 ARE THE POSITIVE AND NEGATIVE "TAILS" OF THE
C     UPWASH PROFILE THAT APPROACH ZERO AS Z APPROACHES INFINITY. THEY
C     ARE USED IN THE "ALIASING" STEP (DESCRIBED IN REF. 13), NECESSARY
C     FOR SUBSEQUENT COMPUTATION OF FAST FOURIER TRANSFORMS
      TAIL1=0.0
      TAIL2=0.0
      DO 150 I=1,41
         FJ=I-21
         IF (FJ.EQ.0) GO TO 150
         Z1=(FJ*VRTSEP)+Z
```

```
      Z2=(FJ*VRTSEP)-Z
      TAIL1=TAIL1+GAMMA/(2.0*PI*Z1)
      TAIL2=TAIL2+GAMMA/(2.0*PI*Z2)
150   CONTINUE
      W(M)=CMPLX(-VRTVEL,0.0)+CMPLX(-TAIL1,0.0)
      W(N-M+2)=CMPLX(+VRTVEL,0.0)+CMPLX(-TAIL2,0.0)
900   CONTINUE
      RETURN
      END
```

```
      SUBROUTINE LIFT
C     SUBROUTINE LIFT COMPUTES THE UNSTEADY LIFT ON THE BLADE BY
C     EVALUATING THE INVERSE FOURIER TRANSFORM OF LO, THE COMPLEX LIFT
C     AMPLITUDE. LO IS EXPRESSED AS A FUNCTION OF AERODYNAMIC FREQUENCY
C     SBAR. LIFT IS EXPRESSED AS A FUNCTION OF RETARDED TIME TP,
C     WHERE TP=T-X/UC. UC IS THE PHASE VELOCITY OF THE LIFT
C     PATTERN, UC=U/TAN(LAMBDA)
C     VALUES ARE RETURNED IN COMPLEX ARRAY C.
      COMPLEX*8 C(2048),W(2048),CL,T,W0,L0,P,V
      COMPLEX*8 CMPLX,CEXP
      REAL L,LAMBDA,MACH,VTHET(1024),VR(1024)
      COMMON W,C,VR,R,THETA,PSI,LAMBDA,OMEGA,GAMMA,GAMMA0,MACH,RHO,S0,
     &       B0,U,H,PI,UFLO,
     &       COSLAM,TANLAM,COTHET,COSPSI,
     &       DS,DSBAR,DT,DTP,DELZ,DR,
     &       N,N2,N4
      DO 177 M=1,N
      C(M)=CMPLX(0.0,0.0)
177   CONTINUE
      A=2.0*PI*RHO*(U**2)*B0
      DTP=(2.0*PI)/(FLOAT(N)*DSBAR)
      TP0=DTP*FLOAT(N)/2.
      DO 100 M=2,N2
      FM=M-1
      DO 200 J=1,2
      IF (J.EQ.2) FM=-FM
      SBAR=FM*DSBAR
      CL=T(SBAR/COSLAM,LAMBDA)
      IF (J.EQ.1) W0=W(M)
      IF (J.EQ.2) W0=W(N-M+2)
      L0=A*CL*W0
      L0=L0*CEXP(CMPLX(0.0,SBAR*TP0))
      IF (CABS(L0).LT.UFLO) GO TO 500
      IF (J.EQ.1) C(M)=L0
      IF (J.EQ.2) C(N-M+2)=L0
200   CONTINUE
```

```
 100  CONTINUE
C     FOURT IS A FAST FOURIER TRANSFORM SUBROUTINE
 500  CALL FOURT(C,N,+1,-1,+1,WORK)
      DO 300 M=1,N
      C(M)=DSBAR*C(M)
 300  CONTINUE
      RETURN
      END
```

```
      SUBROUTINE SOUND
C     SUBROUTINE SOUND COMPUTES THE FARFIELD PRESSURE SIGNAL BY
C     EVALUATING THE INVERSE FOURIER TRANSFORM OF P, THE FREQUENCY
C     SPECTRUM OF THE FARFIELD SIGNAL. P IS EXPRESSED AS A FUNCTION OF
C     OBSERVED FREQUENCY S. THE FARFIELD PRESSURE IS EXPRESSED AS A
C     FUNCTION OF TIME,T. OBSERVED FREQUENCY S IS RELATED TO
C     AERODYNAMIC FREQUENCY SBAR BY SBAR=S*(1-MACH*COS(THETA)*COS(PSI))
C     VALUES ARE RETURNED IN COMPLEX ARRAY C
      COMPLEX*8 C(2048),W(2048),CL,T,WO,LO,P,V,VANLYT
      COMPLEX*8 CMPLX,CEXP
      REAL L,LAMBDA,MACH,VTHET(1024),VR(1024)
      COMMON W,C,VR,R,THETA,PSI,LAMBDA,OMEGA,GAMMA,GAMMA0,MACH,RHO,S0,
     &       B0,U,H,PI,UFLO,
     &       COSLAM,TANLAM,COTHET,COSPSI,
     &       DS,DSBAR,DT,DTP,DELZ,DR,
     &       N,N2,N4
      DO 177 M=1,N
      C(M)=CMPLX(0.0,0.0)
177   CONTINUE
      A=2.0*PI*RHO*(U**2)*B0
      B=(MACH*S0)/(2.0*PI*R)
      X=MACH*COTHET*COSPSI
      Y=1.0-X
      DS=DSBAR/Y
      DT=(2.0*PI)/(FLOAT(N)*DS)
      T0=DT*FLOAT(N)/4.
      DO 400 M=2,N2
      FM=M-1
      DO 500 J=1,2
      IF (J.EQ.2) FM=-FM
      S=FM*DS
      SBAR=FM*DSBAR
      CL=T(SBAR/COSLAM,LAMBDA)
      IF (J.EQ.1) WO=W(M)
      IF (J.EQ.2) WO=W(N-M+2)
      LO=A*CL*WO
```

```
      E=S0*S*((TANLAM*Y)-X)
      DIREC=SIN(THETA)*SIN(E)/E
      P=B*L0*S*DIREC*CMPLX(0.0,1.0)
      P=P*CEXP(CMPLX(0.0,S*T0))
      IF (CABS(P).LT.UFLO) GO TO 700
      IF (J.EQ.1) C(M)=P
      IF (J.EQ.2) C(N-M+2)=P
  500 CONTINUE
  400 CONTINUE
C     FOURT IS A FAST FOURIER TRANSFORM SUBROUTINE
  700 CALL FOURT(C,N,+1,-1,+1,WORK)
      DO 600 M=1,N
      C(M)=DS*C(M)
  600 CONTINUE
      RETURN
      END
```

```
      SUBROUTINE TRNSFM
C     TRNSFM COMPUTES THE FOURIER TRANSFORM OF VERTICAL VELOCITY
C     W IN TERMS OF WAVENUMBER SIGMA, THEN EXPRESSES THE TRANSFORM
C     AS A FUNCTION OF AERODYNAMIC FREQUENCY SBAR,
C     WHERE SBAR=SIGMA*COS(LAMBDA)
      COMPLEX*8 C(2048),W(2048),CL,T,W0,L0,P
      COMPLEX*8 CMPLX,CEXP
      REAL L,LAMBDA,MACH,VTHET(1024),VR(1024)
      COMMON W,C,VR,R,THETA,PSI,LAMBDA,OMEGA,GAMMA,GAMMA0,MACH,RHO,S0,
     &       B0,U,H,PI,UFLO,
     &       COSLAM,TANLAM,COTHET,COSPSI,
     &       DS,DSBAR,DT,DTP,DELZ,DR,
     &       N,N2,N4
C     FOURT IS A FAST FOURIER TRANSFORM SUBROUTINE
      CALL FOURT(W,N,+1,-1,+1,WORK)
      DO 100 M=1,N
      W(M)=W(M)*(DELZ/(2.0*PI))
  100 CONTINUE
      DSIG=(2.0*PI)/(FLOAT(N)*DELZ)
      DSBAR=DSIG*COSLAM
      DO 200 M=1,N
      W(M)=W(M)/COSLAM
  200 CONTINUE
      RETURN
      END
```

```
      FUNCTION FMIN(C,N)
C     FMIN IS THE MINIMUM REAL VALUE CONTAINED IN A COMPLEX ARRAY C OF
C     LENGTH N
      COMPLEX*8 C(N)
      P=0.0
      DO 100 M=1,N
      Q=REAL(C(M))
      IF (Q.LT.P) P=Q
  100 CONTINUE
      FMIN=P
      RETURN
      END
C
      FUNCTION FMAX(C,N)
C     FMAX IS THE MAXIMUM REAL VALUE CONTAINED IN A COMPLEX ARRAY C OF
C     LENGTH N
      COMPLEX*8 C(N)
      P=0.0
      DO 100 M=1,N
      Q=REAL(C(M))
      IF (Q.GT.P) P=Q
  100 CONTINUE
      FMAX=P
      RETURN
      END
```

```
      SUBROUTINE DB
C     DB COMPUTES THE INTENSITY OF THE ACOUSTIC SIGNAL IN DECIBELS
      COMPLEX*8 C(2048),W(2048),CL,T,WO,LO
      COMPLEX*8 CMPLX,CEXP
      REAL L,LAMBDA,MACH,VTHET(1024),VR(1024)
      COMMON W,C,VR,R,THETA,PSI,LAMBDA,OMEGA,GAMMA,GAMMAO,MACH,RHO,SO,
     &       BO,U,H,PI,UFLO,
     &       COSLAM,TANLAM,COTHET,COSPSI,
     &       DS,DSBAR,DT,DTP,DELZ,DR,
     &       N,N2,N4
      DELP=FMAX(C,N)-FMIN(C,N)
      P=(DELP/2.0)*47.88
      PREF=0.00002
      DBL=20.0*ALOG10(P/PREF)
      WRITE(6,99) H,DBL
 99   FORMAT(F10.2,F10.2)
      RETURN
      END
```

```
      COMPLEX FUNCTION T(SIGMA,LAMBDA)
C     T IS THE LIFT TRANSFER FUNCTION GIVEN BY FILOTAS THEORY
C     SIGMA IS A DIMENSIONLESS WAVE NUMBER, SIGMA=SBAR/COS(LAMBDA)
      REAL LAMBDA
      COMPLEX*8 E
      COMPLEX*8 CMPLX,CEXP
      SINLAM=SIN(LAMBDA)
      COSLAM=COS(LAMBDA)
      PI=3.1415926
      SIGABS=ABS(SIGMA)
      A=1.0+(0.5*SINLAM)
      B=PI*((PI/2.0)-LAMBDA)*A
      C=1.0+((2.0*PI*SIGABS)*A)
      PHI=COSLAM-(B/C)
      D=1.0+(COSLAM**2)+(PI*SIGABS*SINLAM)
      F=1.0+(PI*SIGABS*D)
      G=F**0.5
      E=CEXP(CMPLX(0.0,-SIGMA*PHI))
      T=E/CMPLX(G,0.0)
      RETURN
      END
```

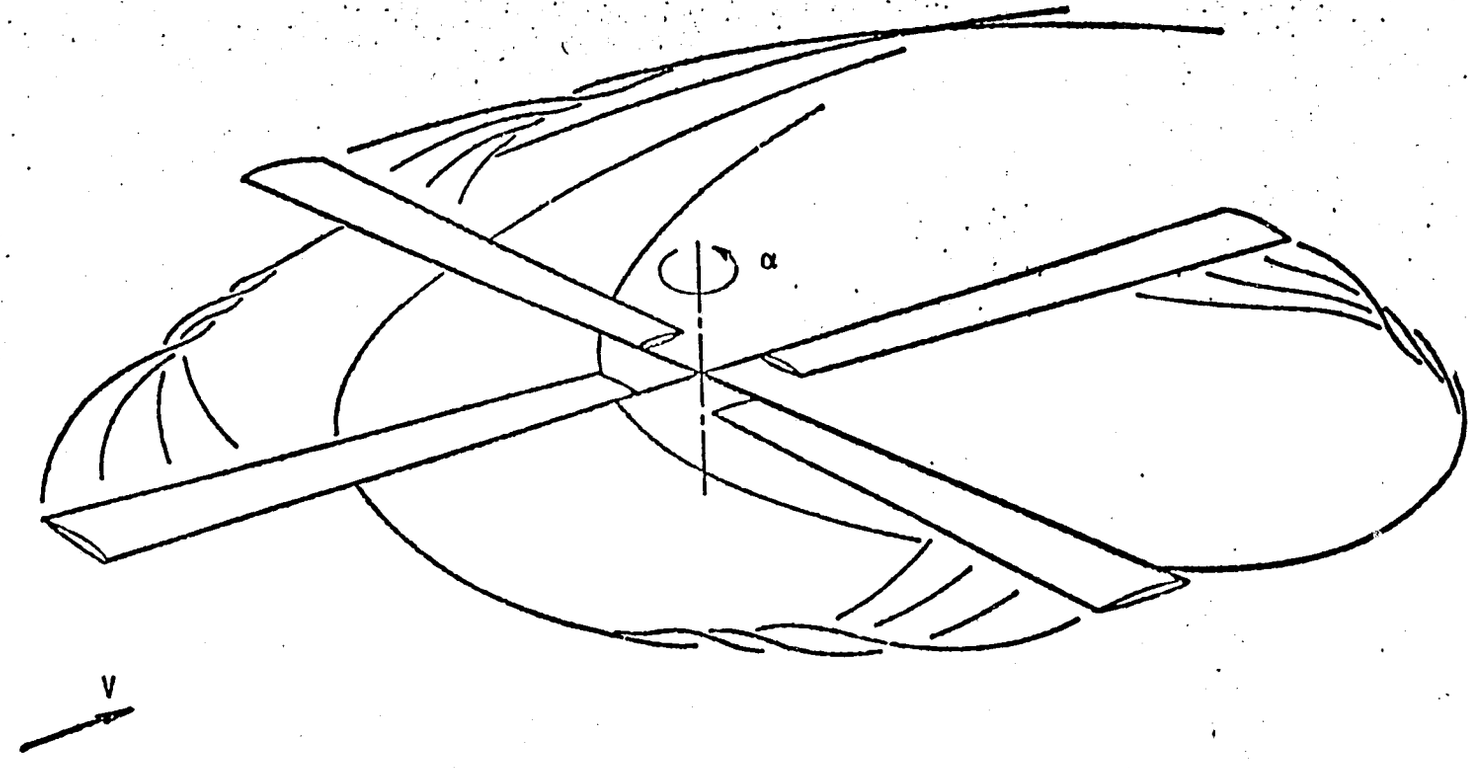

Figure 1. Generation of Helicopter Rotor Tip Vortices (after ref. 4)

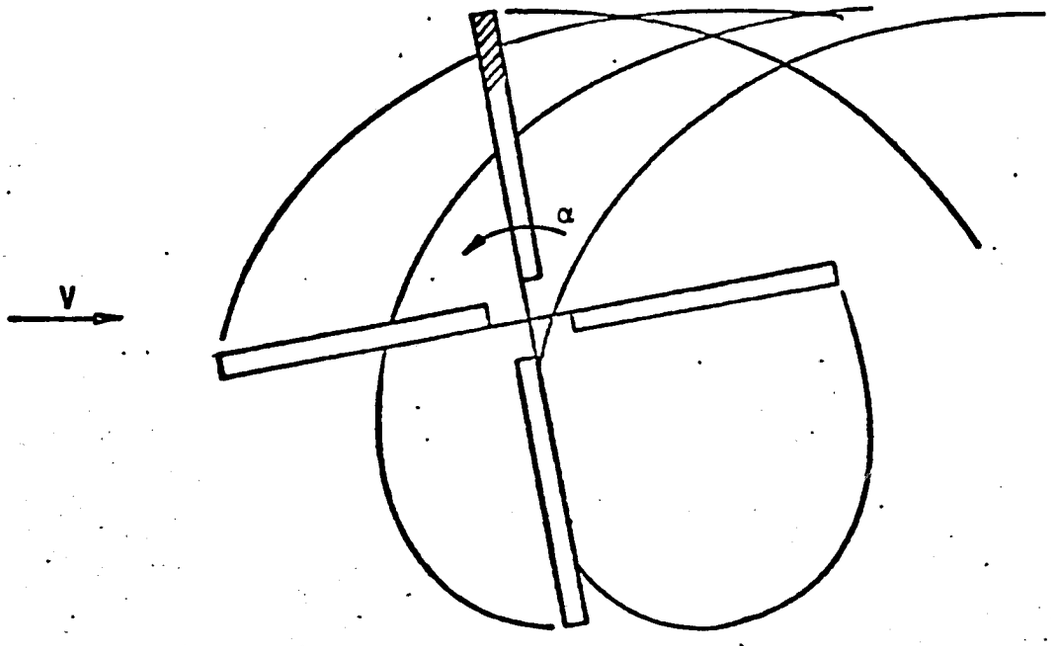

(2a)

important interactions

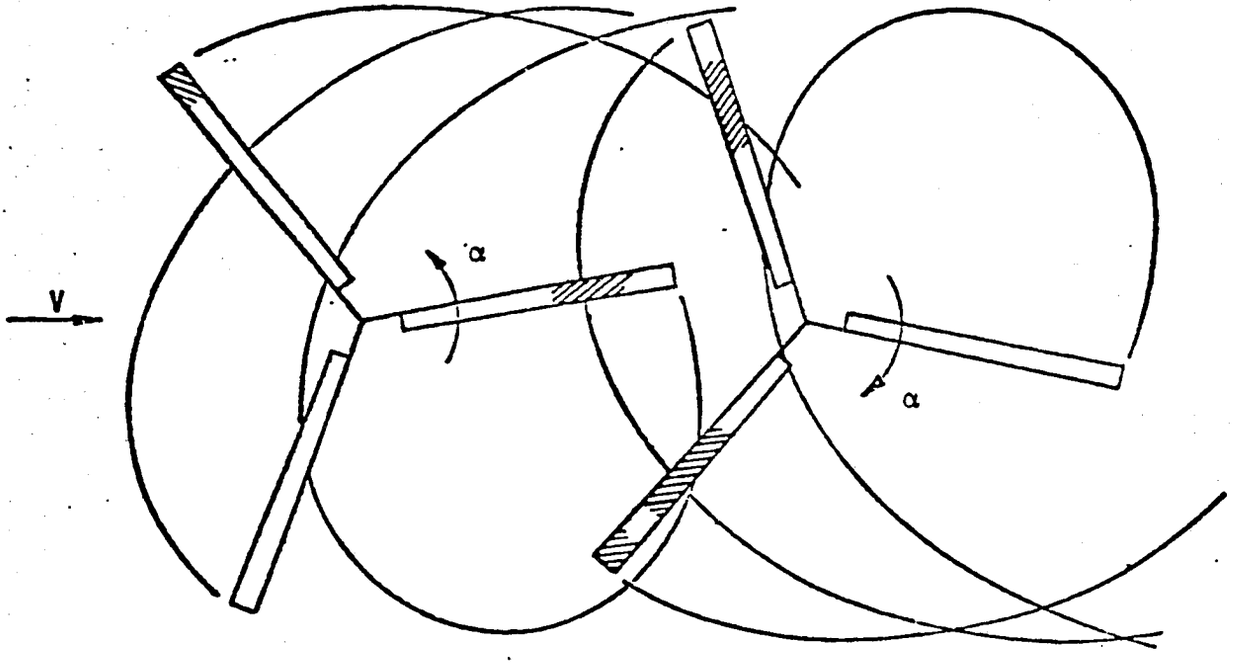

(2b)

Figure 2. Blade/Vortex Interaction for Single and Tandem Rotors (after ref. 3)

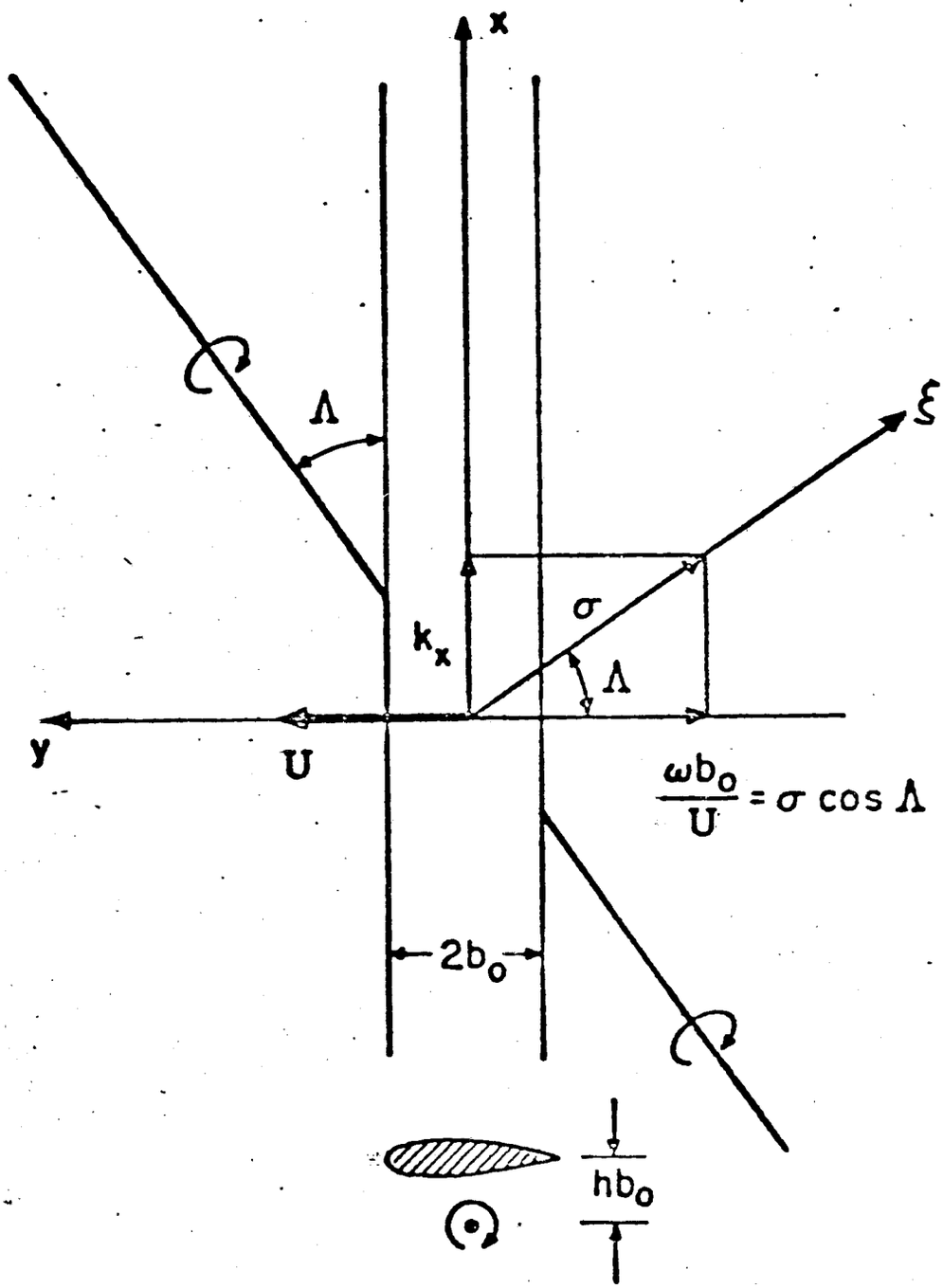

Figure 3. Geometry of Blade/Vortex Interaction (after ref. 3)

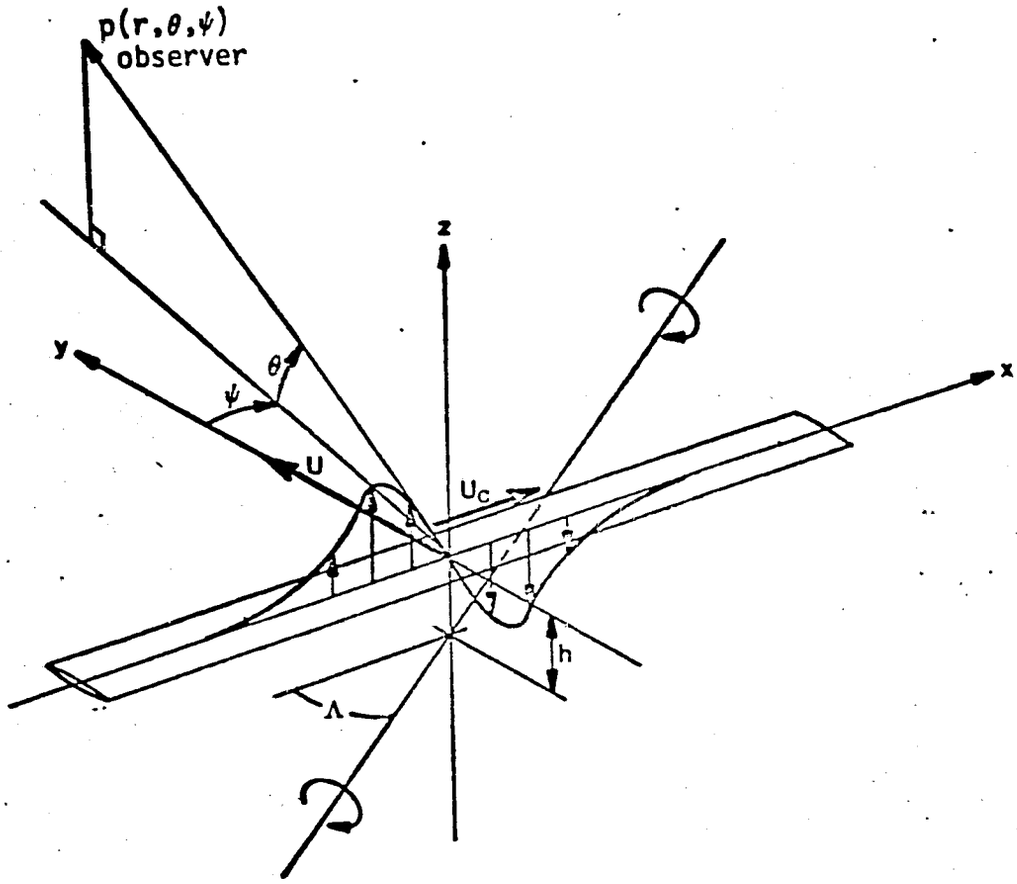

Figure 4. Geometry of Acoustic Model

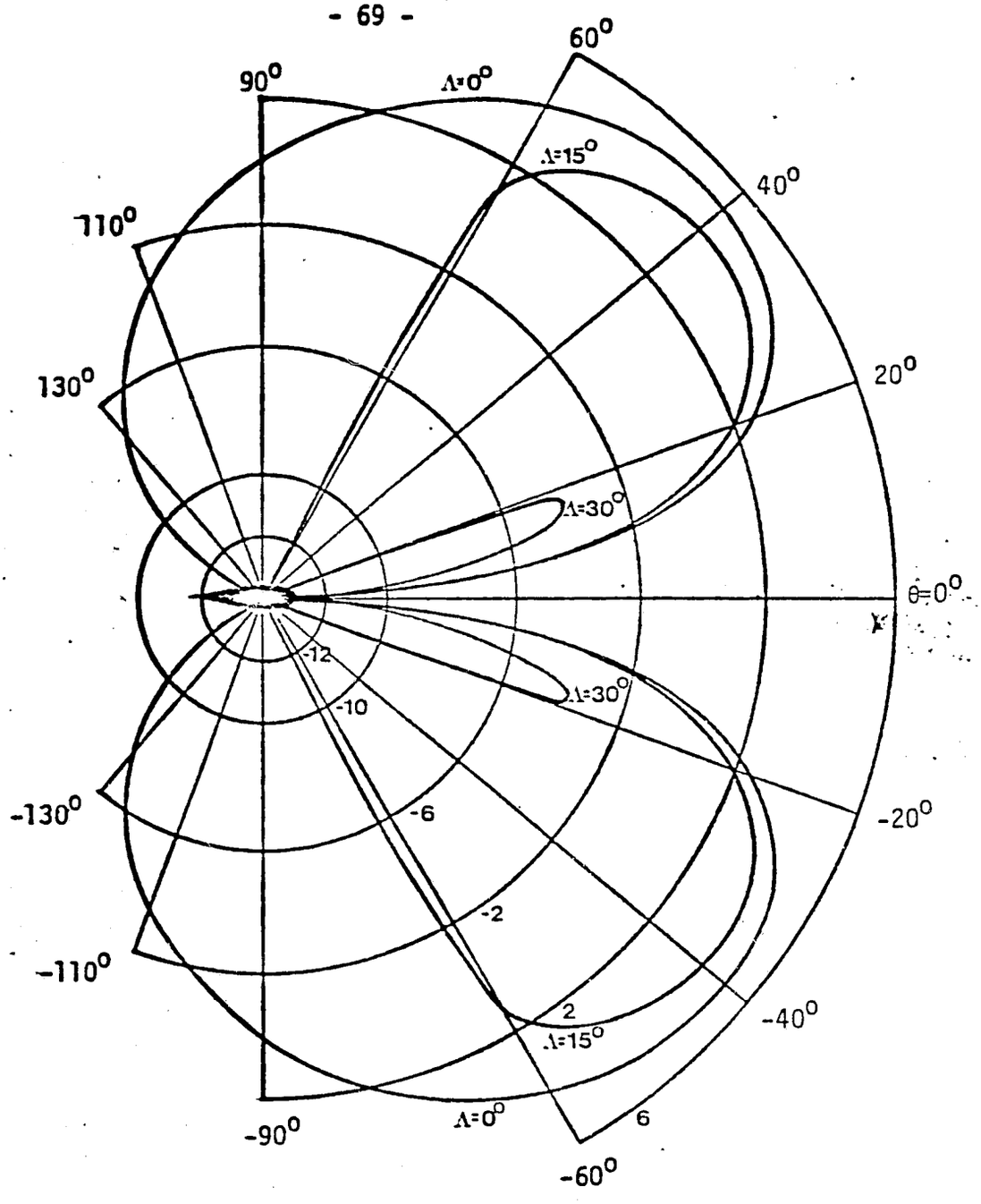

Figure 5. Maximum amplitude of the directivity factor as a function of θ for $ks_o >> 1$; $20\log D(\theta, \psi_{crit})$ for M=.53

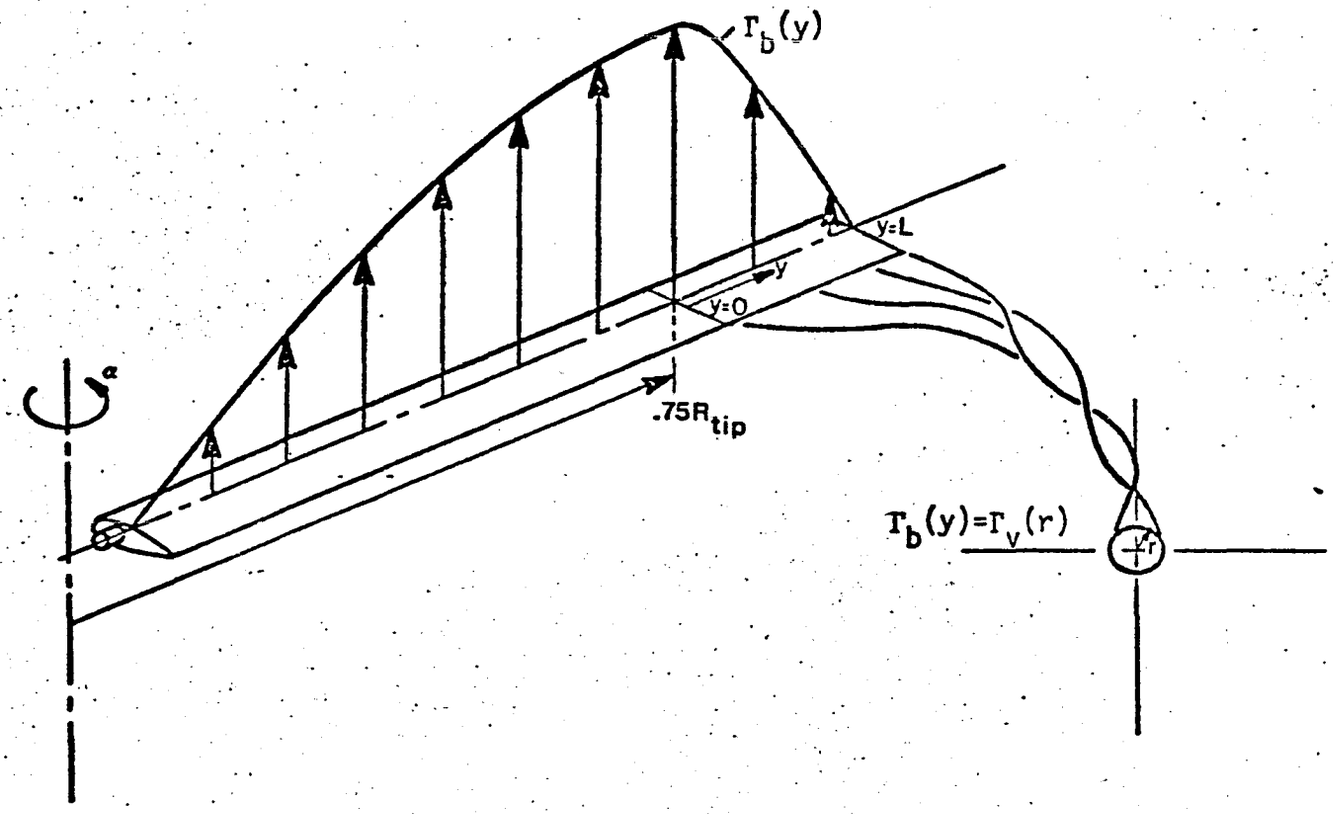

Figure 6. Geometry applied to the Betz vortex rollup model. Maximum loading is assumed at 75% span, so that vorticity shed from the outboard 25% span rolls up into the trailing vortex.

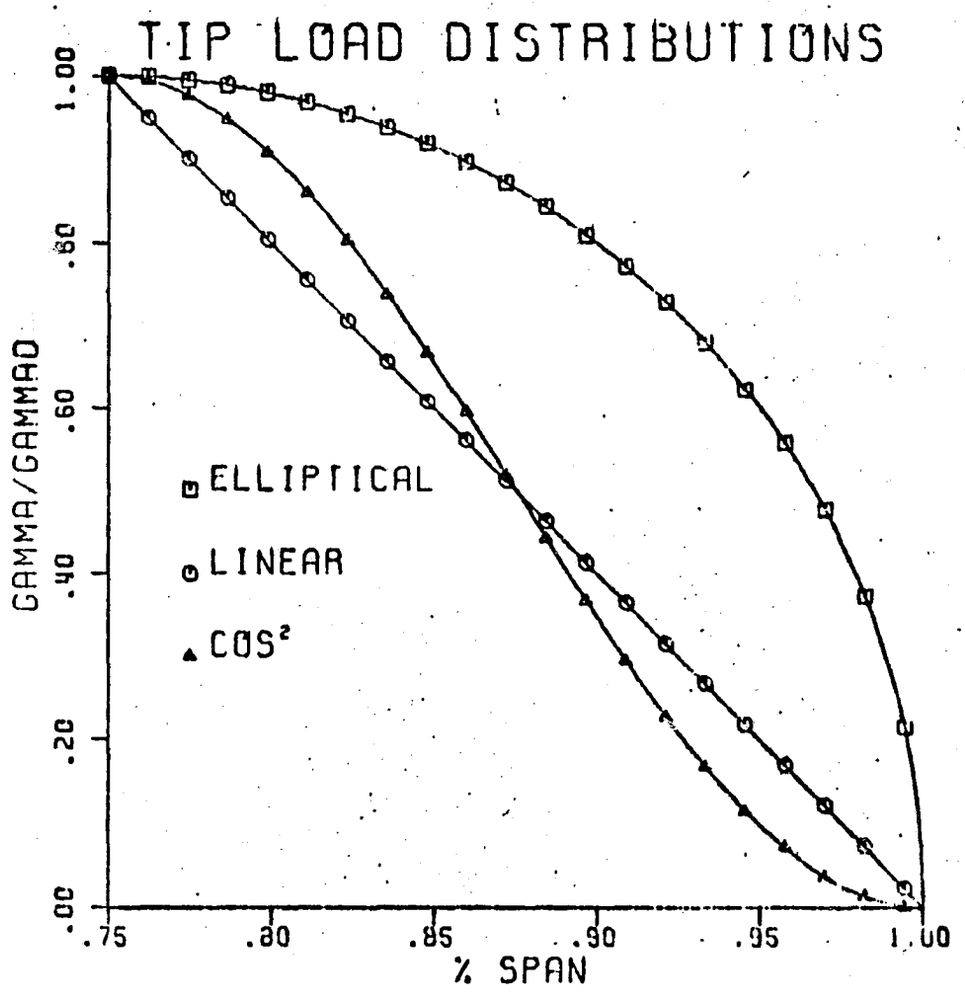
TIP LOAD DISTRIBUTIONS
GAMMA/GAMMAD
1.00
.80
.60
.40
.20
.00
.75
.80
.85
.90
.95
1.00
% SPAN
ELLIPTICAL
LINEAR
COS²

Figure 7

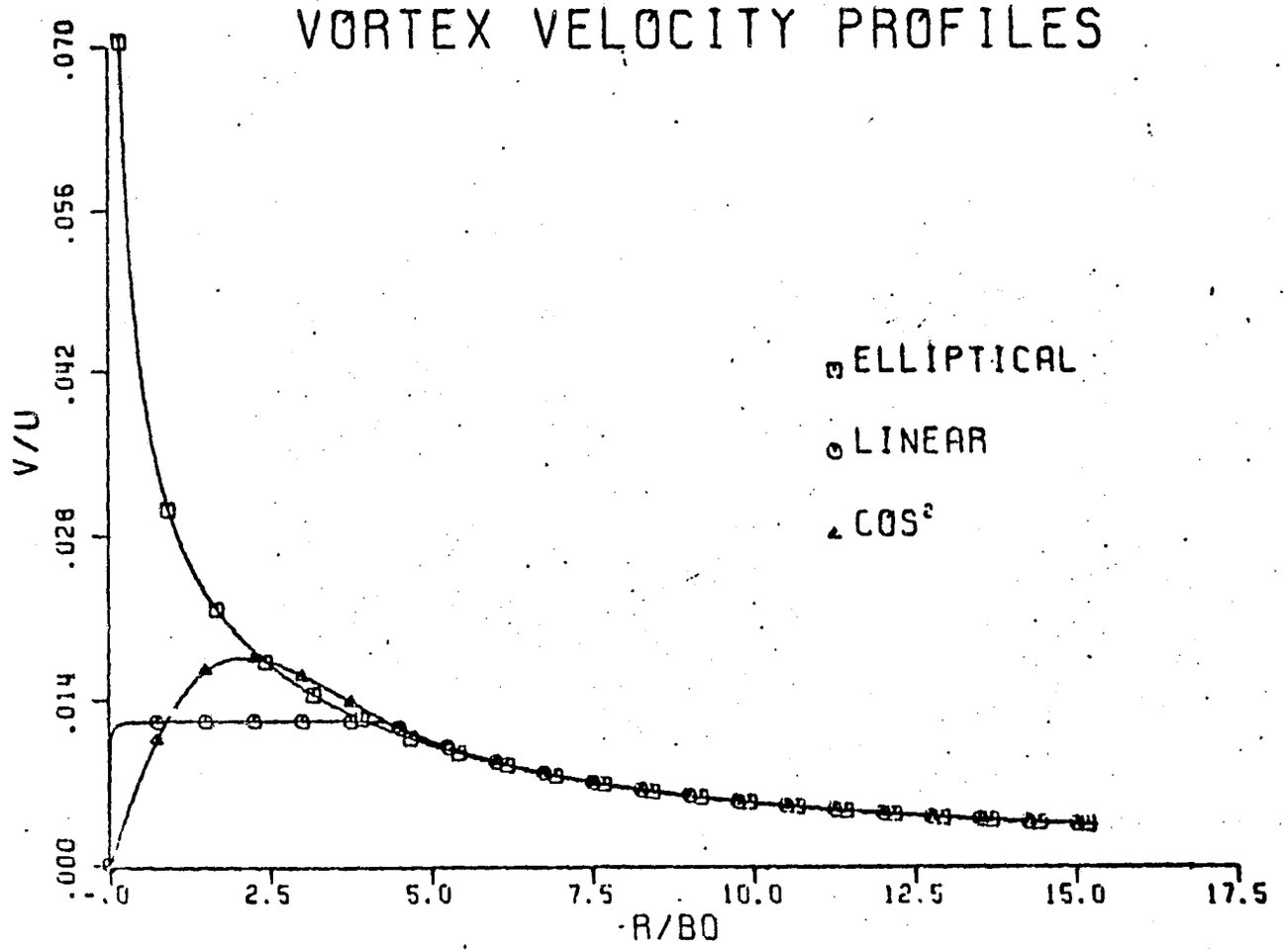
VORTEX VELOCITY PROFILES
V/U
.070
.056
.042
.028
.014
.000
.0
2.5
5.0
7.5
10.0
12.5
15.0
17.5
R/BO
ELLIPTICAL
LINEAR
COS²

Figure 8

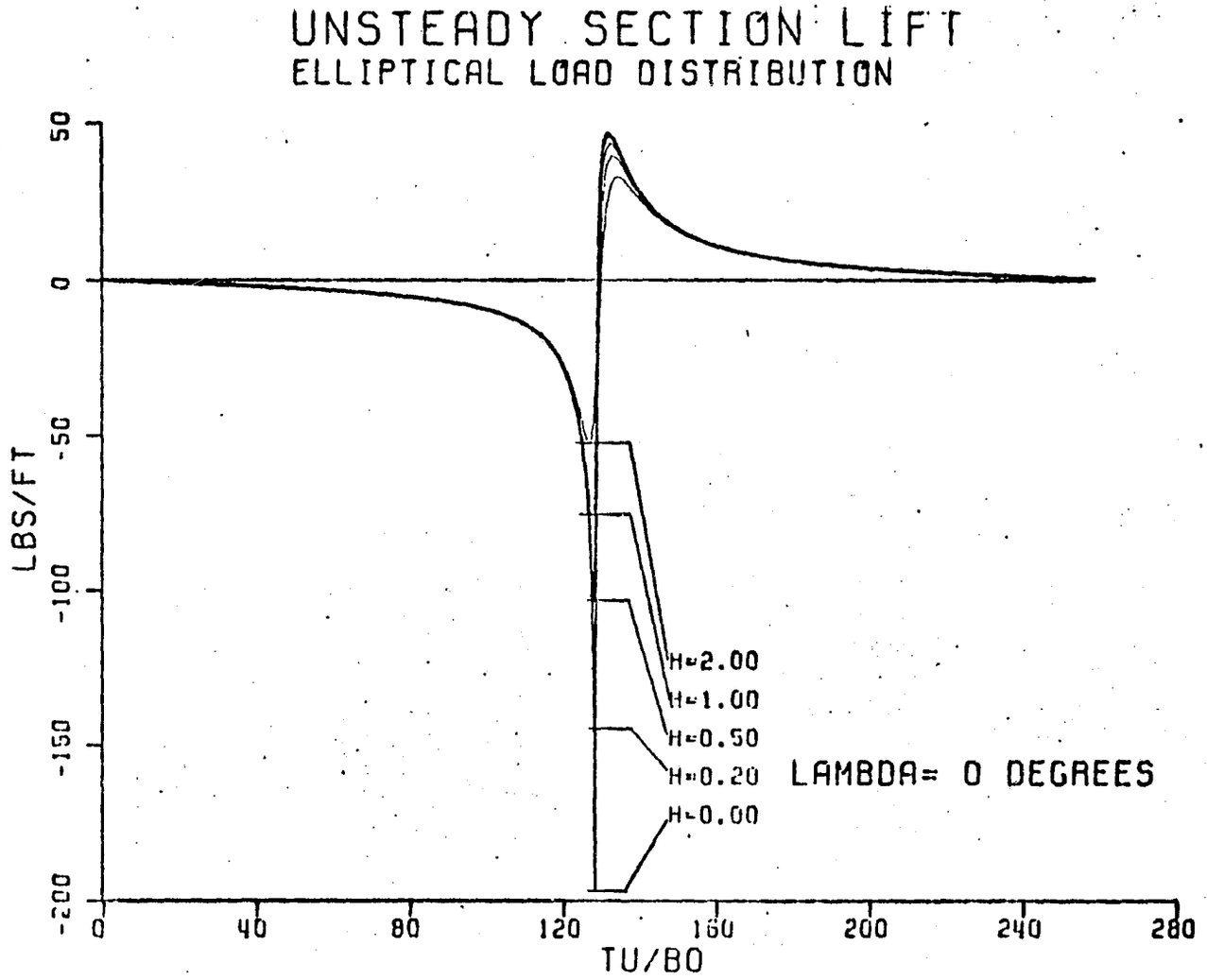
UNSTEADY SECTION LIFT
ELLIPTICAL LOAD DISTRIBUTION
LBS/FT
50
0
-50
-100
-150
-200
0
40
80
120
160
200
240
280
TU/BO
H=2.00
H=1.00
H=0.50
H=0.20
H=0.00
LAMBDA= 0 DEGREES

Figure 9

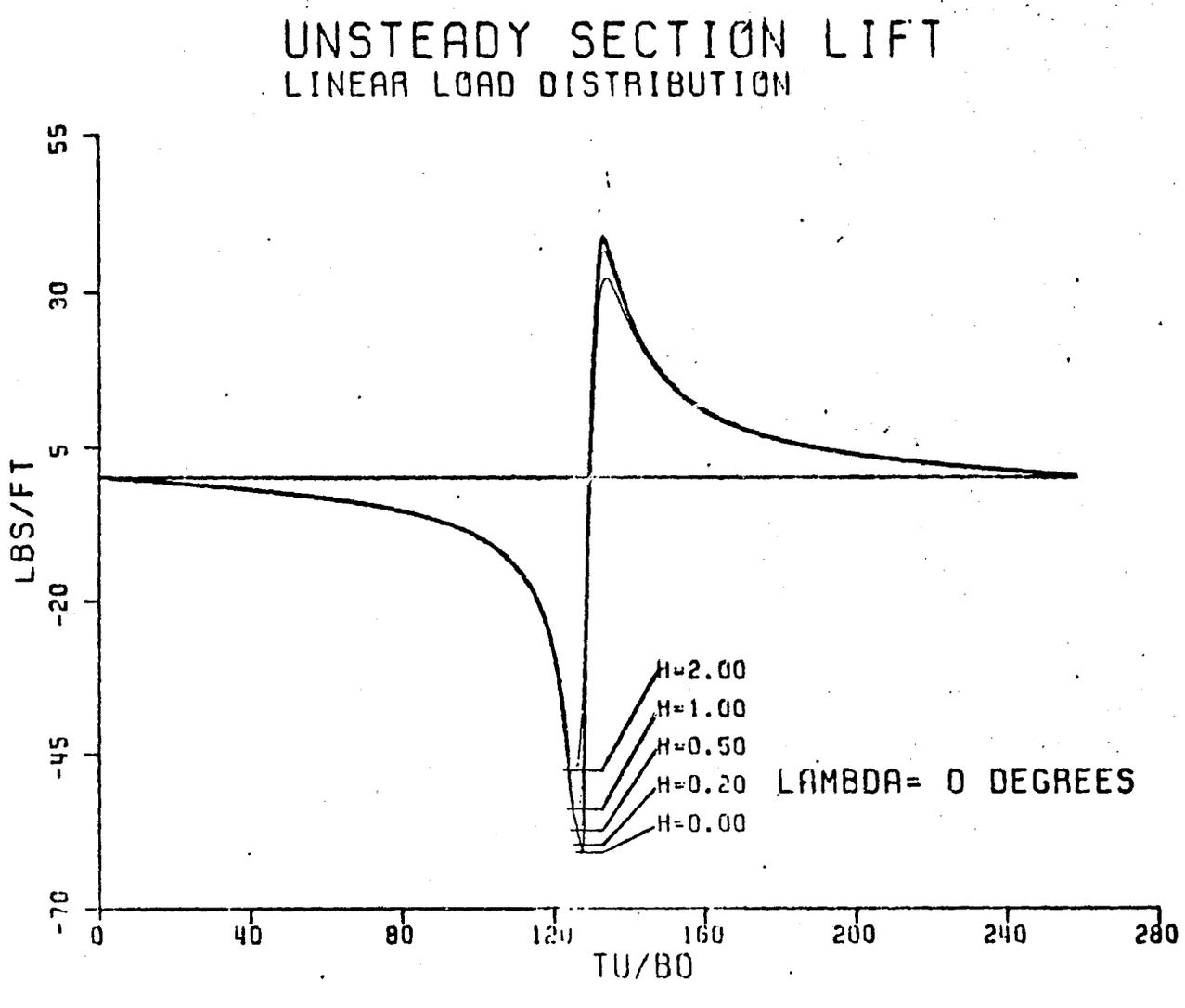
UNSTEADY SECTION LIFT
LINEAR LOAD DISTRIBUTION
LBS/FT
55
30
5
-20
-45
-70
0
40
80
120
160
200
240
280
TU/BO
H=2.00
H=1.00
H=0.50
H=0.20
H=0.00
LAMBDA= 0 DEGREES

Figure 10

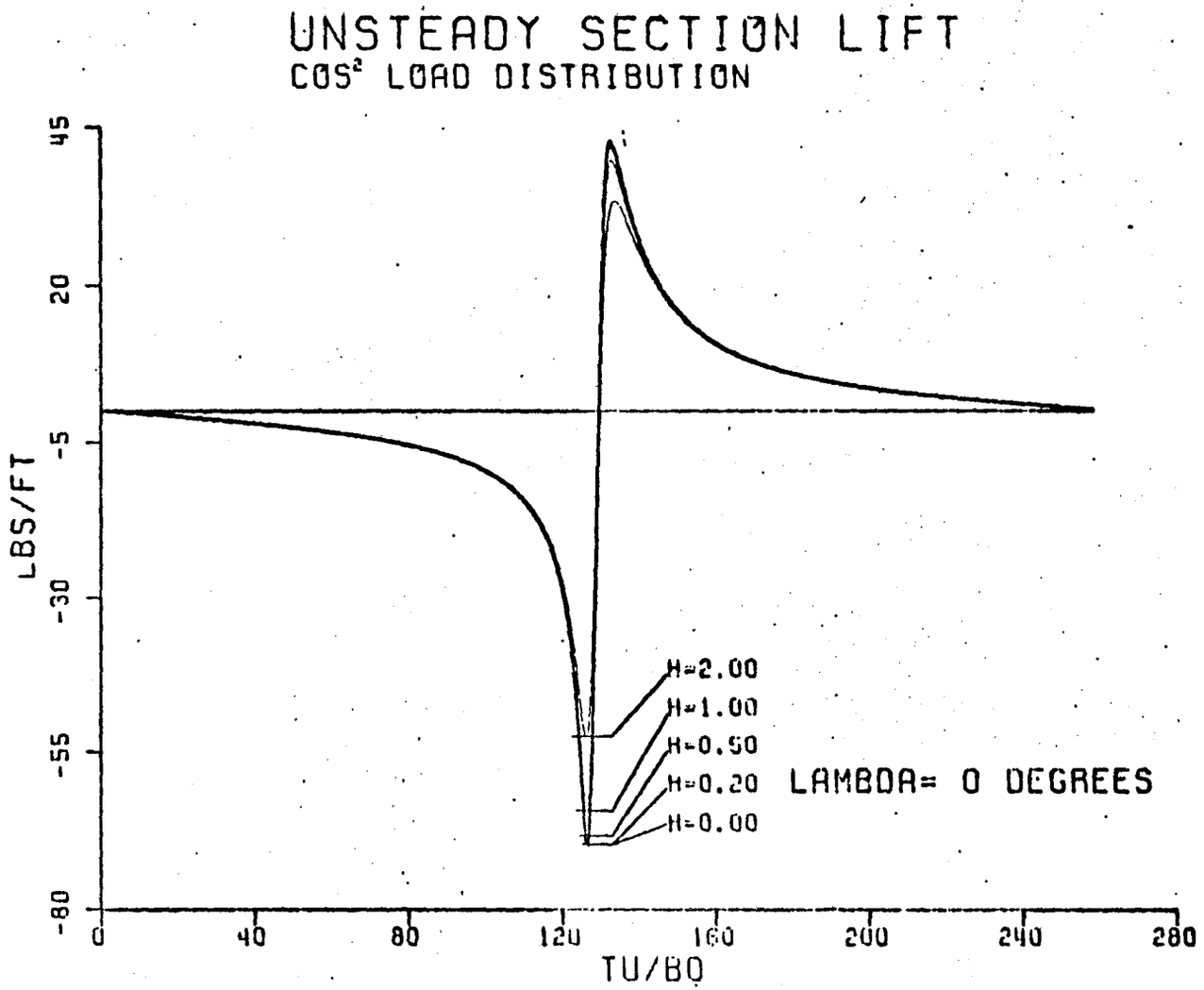
UNSTEADY SECTION LIFT
COS² LOAD DISTRIBUTION
LBS/FT
45
20
-5
-30
-55
-80
0
40
80
120
160
200
240
280
TU/BO
H=2.00
H=1.00
H=0.50
H=0.20
H=0.00
LAMBDA= 0 DEGREES

Figure 11

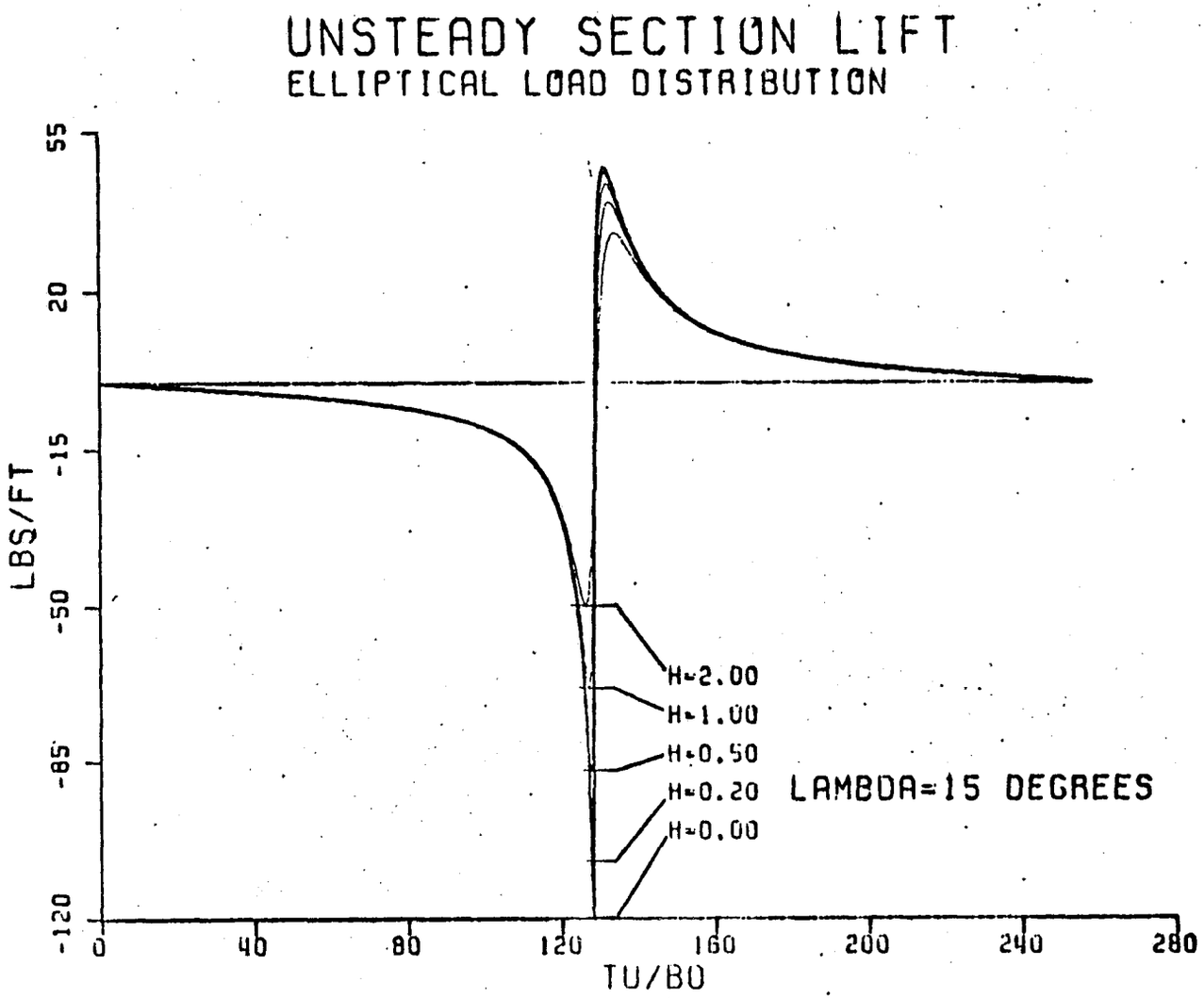
UNSTEADY SECTION LIFT
ELLIPTICAL LOAD DISTRIBUTION
LBS/FT
55
20
-15
-50
-85
-120
0
40
80
120
160
200
240
280
TU/BO
H=2.00
H=1.00
H=0.50
H=0.20
H=0.00
LAMBDA=15 DEGREES

Figure 12

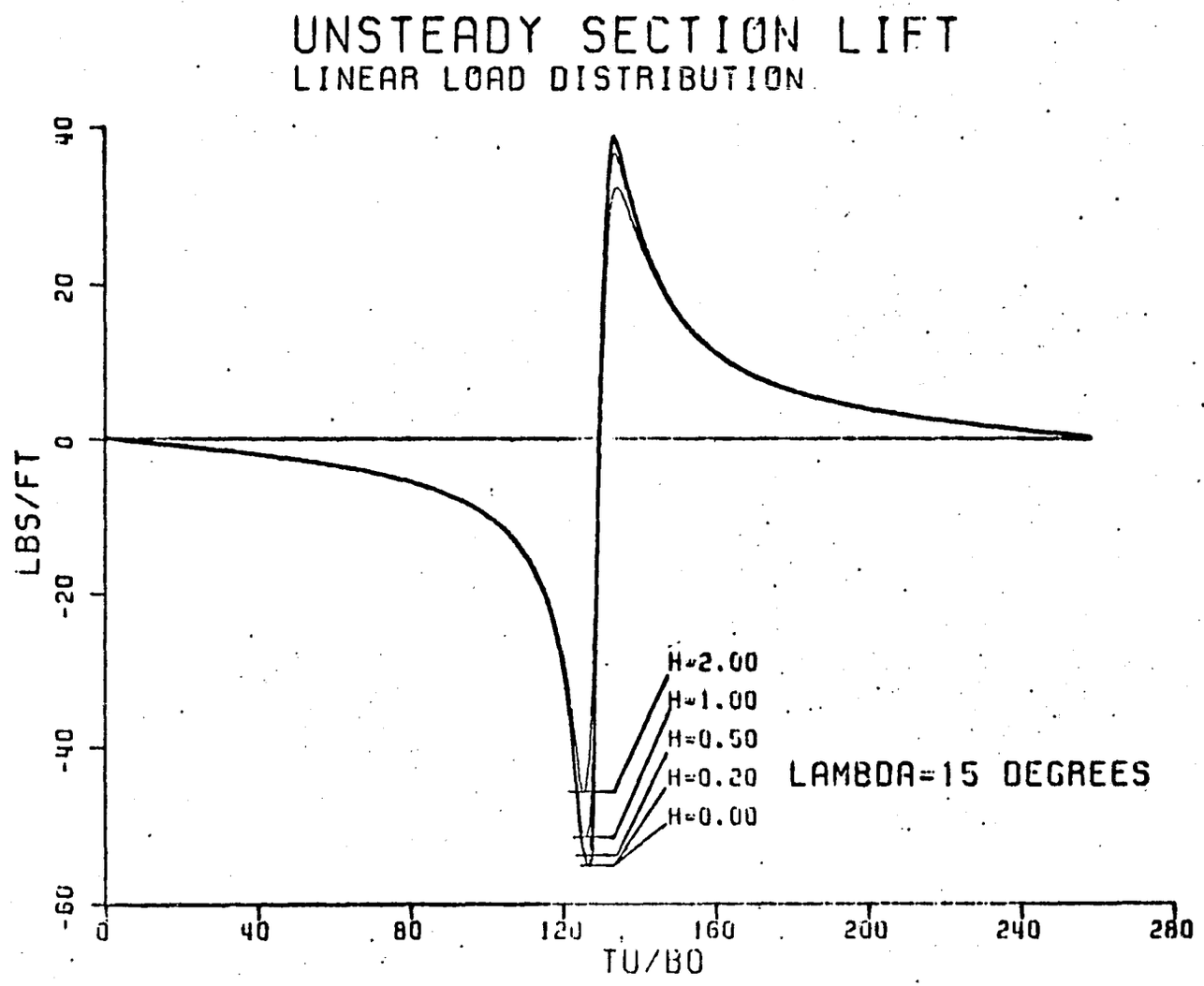
UNSTEADY SECTION LIFT
LINEAR LOAD DISTRIBUTION
LBS/FT
40
20
0
-20
-40
-60
0
40
80
120
160
200
240
280
TU/BO
H=2.00
H=1.00
H=0.50
H=0.20
H=0.00
LAMBDA=15 DEGREES

Figure 13

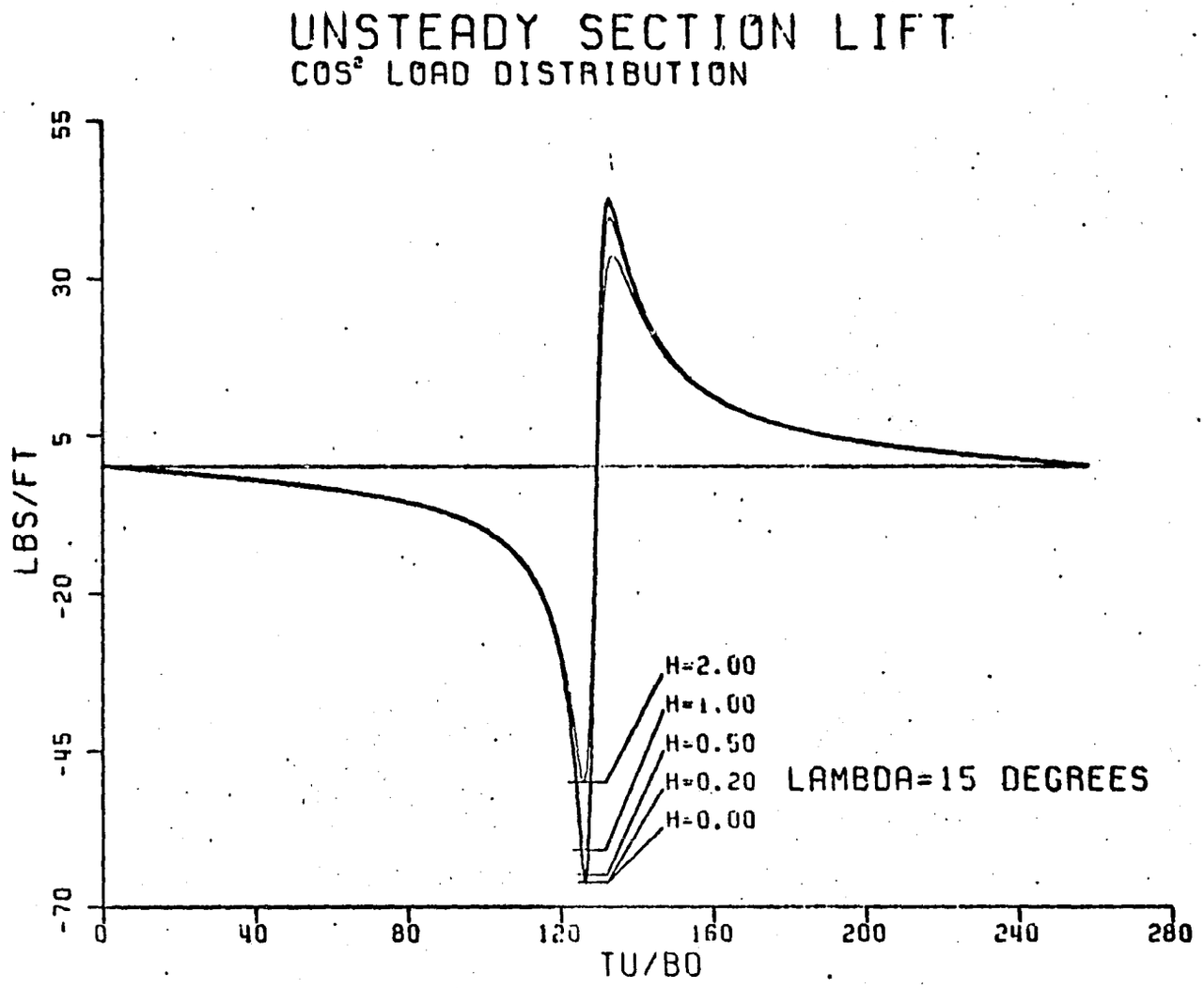
UNSTEADY SECTION LIFT
COS² LOAD DISTRIBUTION
LBS/FT
55
30
5
-20
-45
-70
0
40
80
120
160
200
240
280
TU/BO
H=2.00
H=1.00
H=0.50
H=0.20
H=0.00
LAMBDA=15 DEGREES

Figure 14

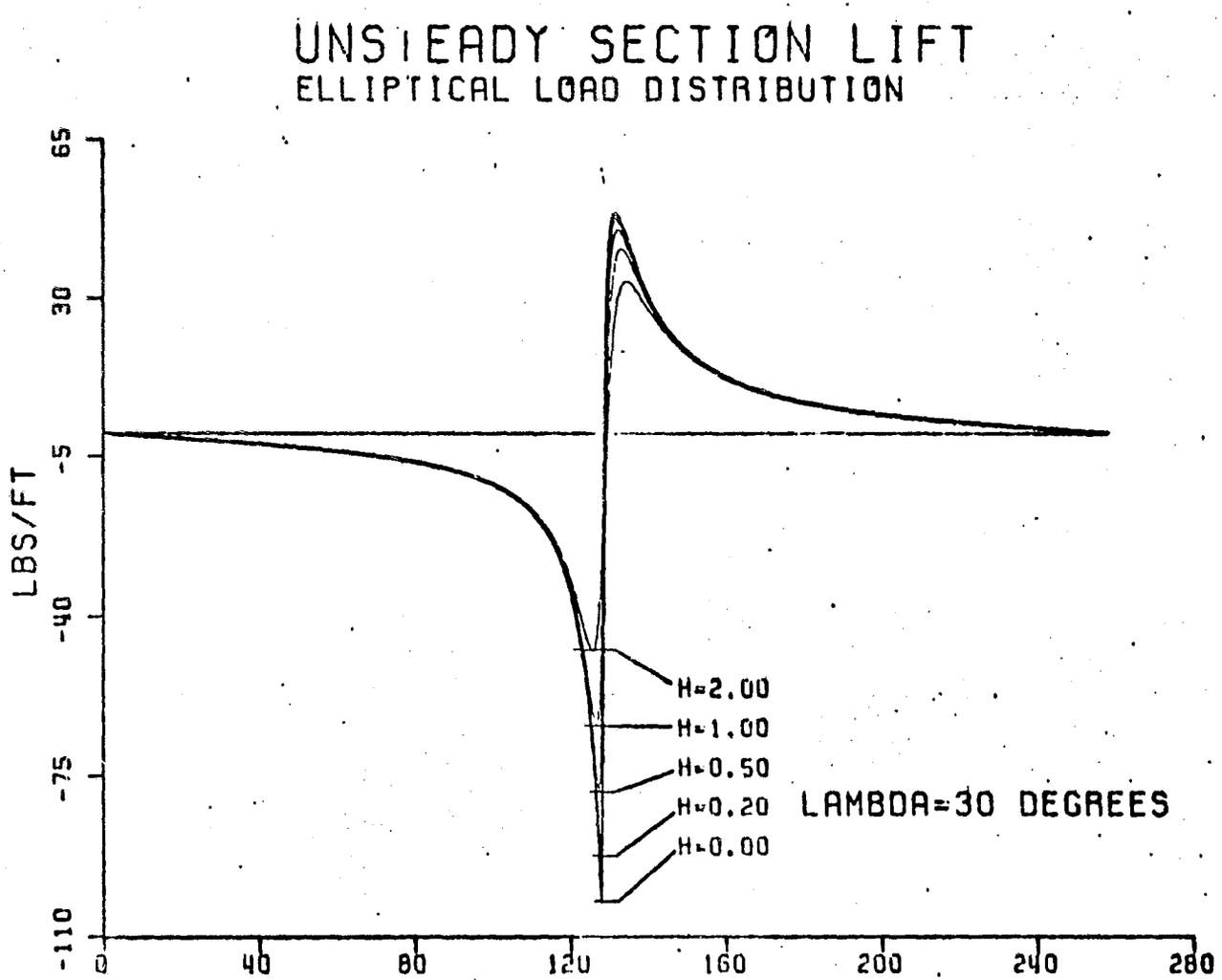
UNSTEADY SECTION LIFT
ELLIPTICAL LOAD DISTRIBUTION
LBS/FT
65
30
-5
-40
-75
-110
0
40
80
120
160
200
240
280
TU/BO
H=2.00
H=1.00
H=0.50
H=0.20
H=0.00
LAMBDA=30 DEGREES

Figure 15

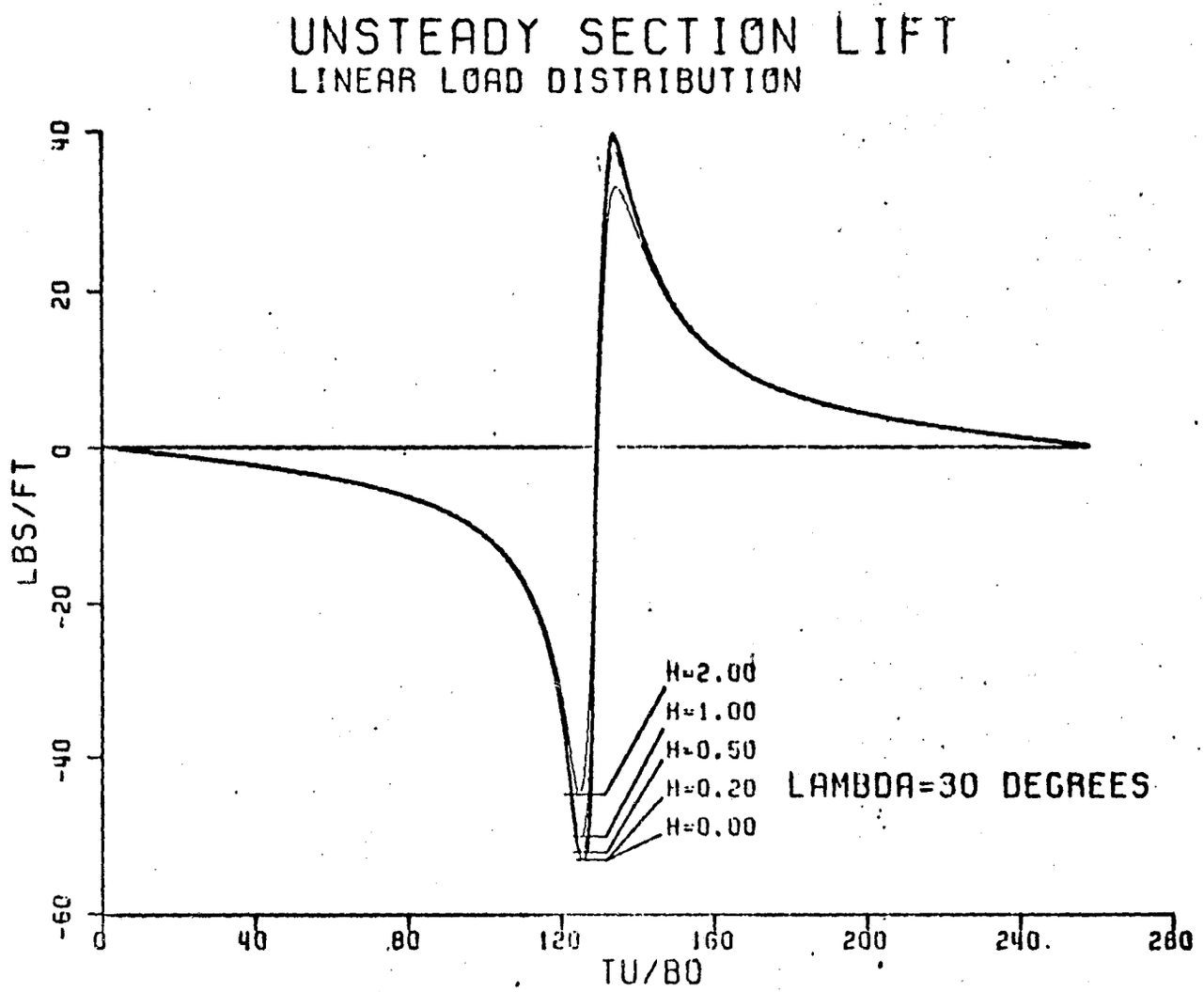
UNSTEADY SECTION LIFT
LINEAR LOAD DISTRIBUTION
LBS/FT
40
20
0
-20
-40
-60
0
40
80
120
160
200
240.
280
TU/BO
H=2.00
H=1.00
H=0.50
H=0.20
H=0.00
LAMBDA=30 DEGREES

Figure 16

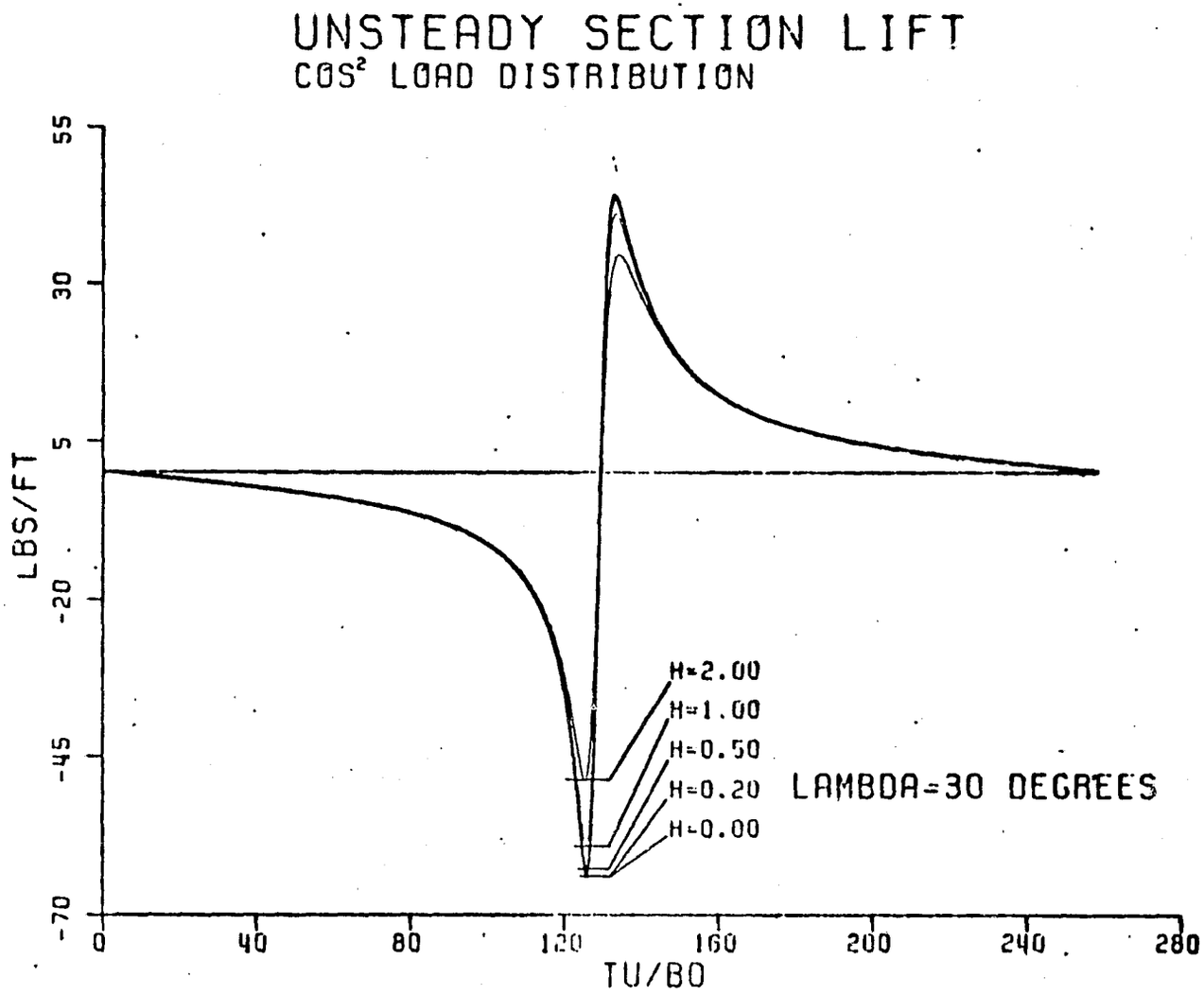
UNSTEADY SECTION LIFT
COS² LOAD DISTRIBUTION
LBS/FT
55
30
5
-20
-45
-70
0
40
80
120
160
200
240
280
TU/BO
H=2.00
H=1.00
H=0.50
H=0.20
H=0.00
LAMBDA=30 DEGREES

Figure 17

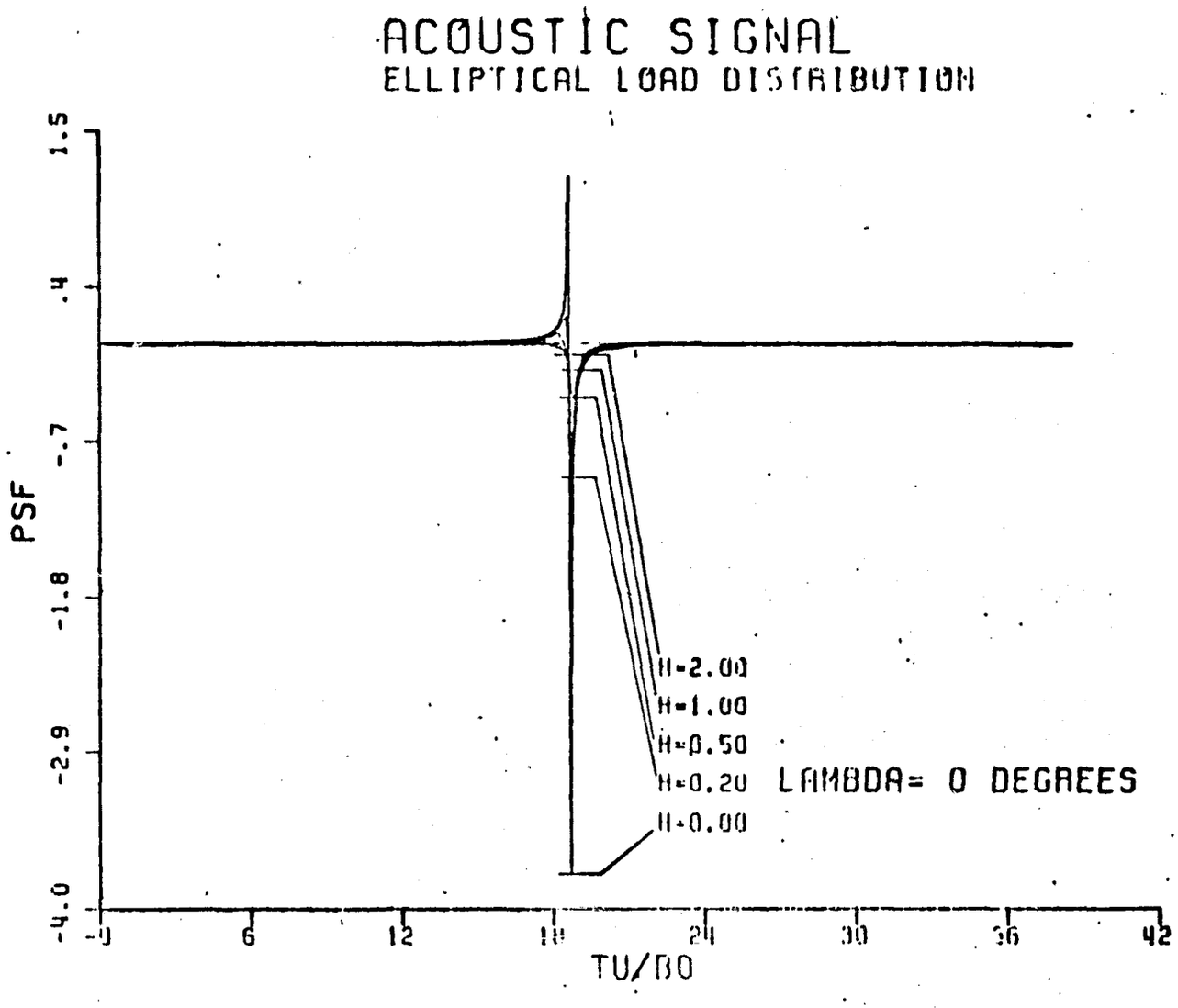
ACOUSTIC SIGNAL
ELLIPTICAL LOAD DISTRIBUTION
PSF
1.5
.4
-.7
-1.8
-2.9
-4.0
0
6
12
18
24
30
36
42
TU/BD
H=2.00
H=1.00
H=0.50
H=0.20
H=0.00
LAMBDA= 0 DEGREES

Figure 18

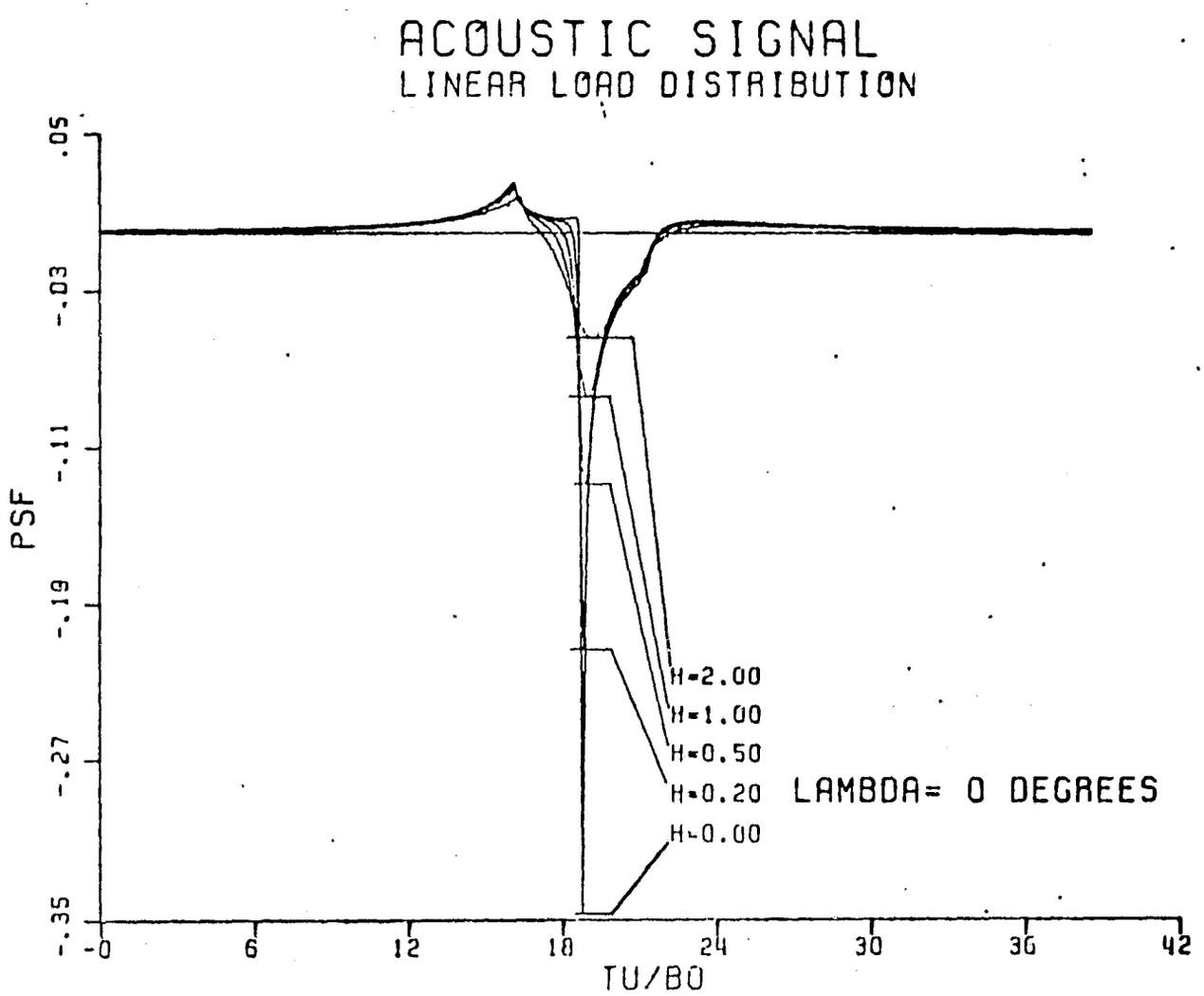
ACOUSTIC SIGNAL
LINEAR LOAD DISTRIBUTION
PSF
.05
-.03
-.11
-.19
-.27
-.35
-0
6
12
18
24
30
36
42
TU/BU
H=2.00
H=1.00
H=0.50
H=0.20
H=0.00
LAMBDA= 0 DEGREES

Figure 19

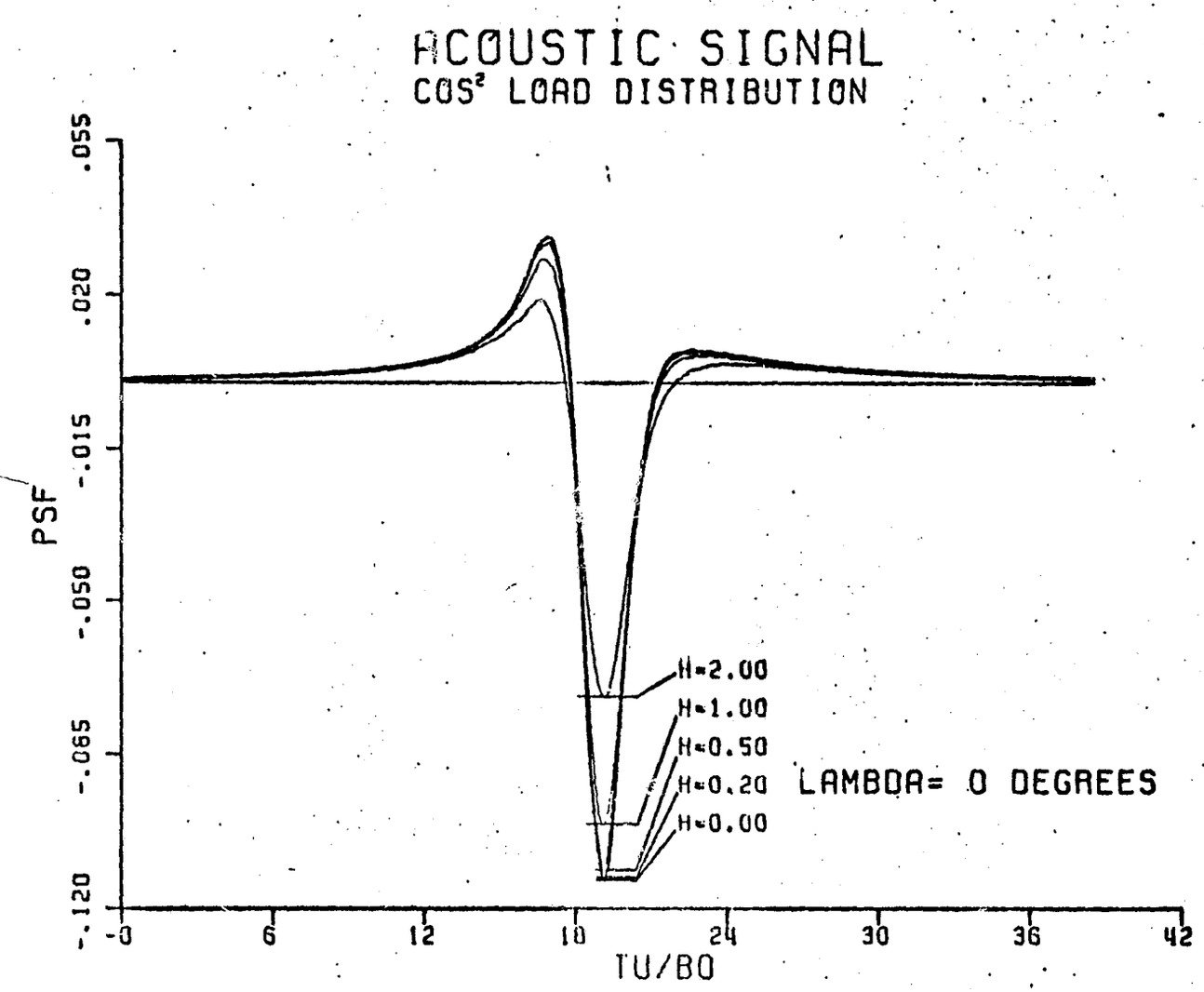
ACOUSTIC SIGNAL
COS² LOAD DISTRIBUTION
PSF
.055
.020
-.015
-.050
-.065
-.120
-0
6
12
18
24
30
36
42
TU/BO
H=2.00
H=1.00
H=0.50
H=0.20
H=0.00
LAMBDA= 0 DEGREES

Figure 20

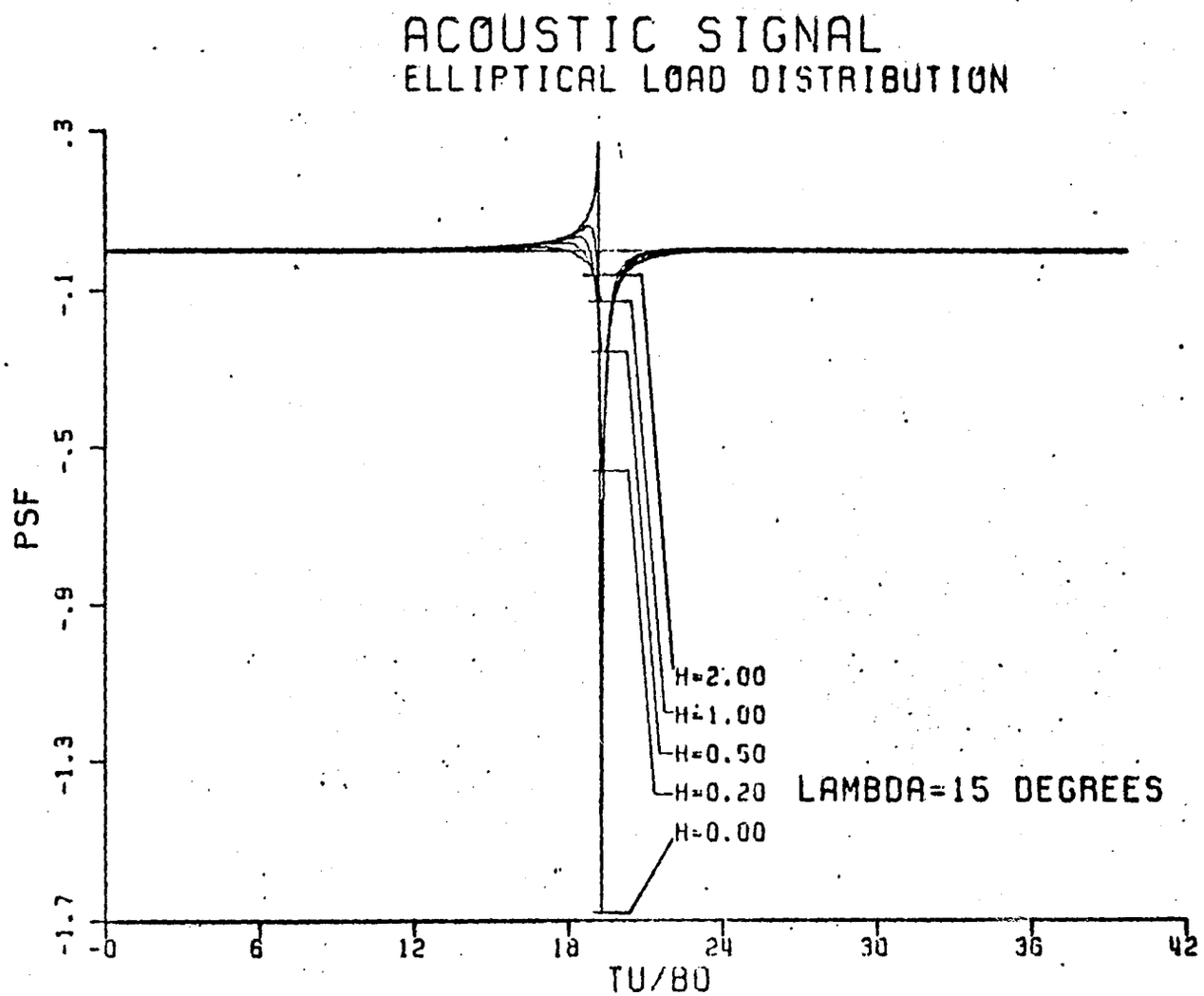
ACOUSTIC SIGNAL
ELLIPTICAL LOAD DISTRIBUTION
PSF
.3
-.1
-.5
-.9
-1.3
-1.7
0
6
12
18
24
30
36
42
TU/80
H=2.00
H=1.00
H=0.50
H=0.20
H=0.00
LAMBDA=15 DEGREES

Figure 21

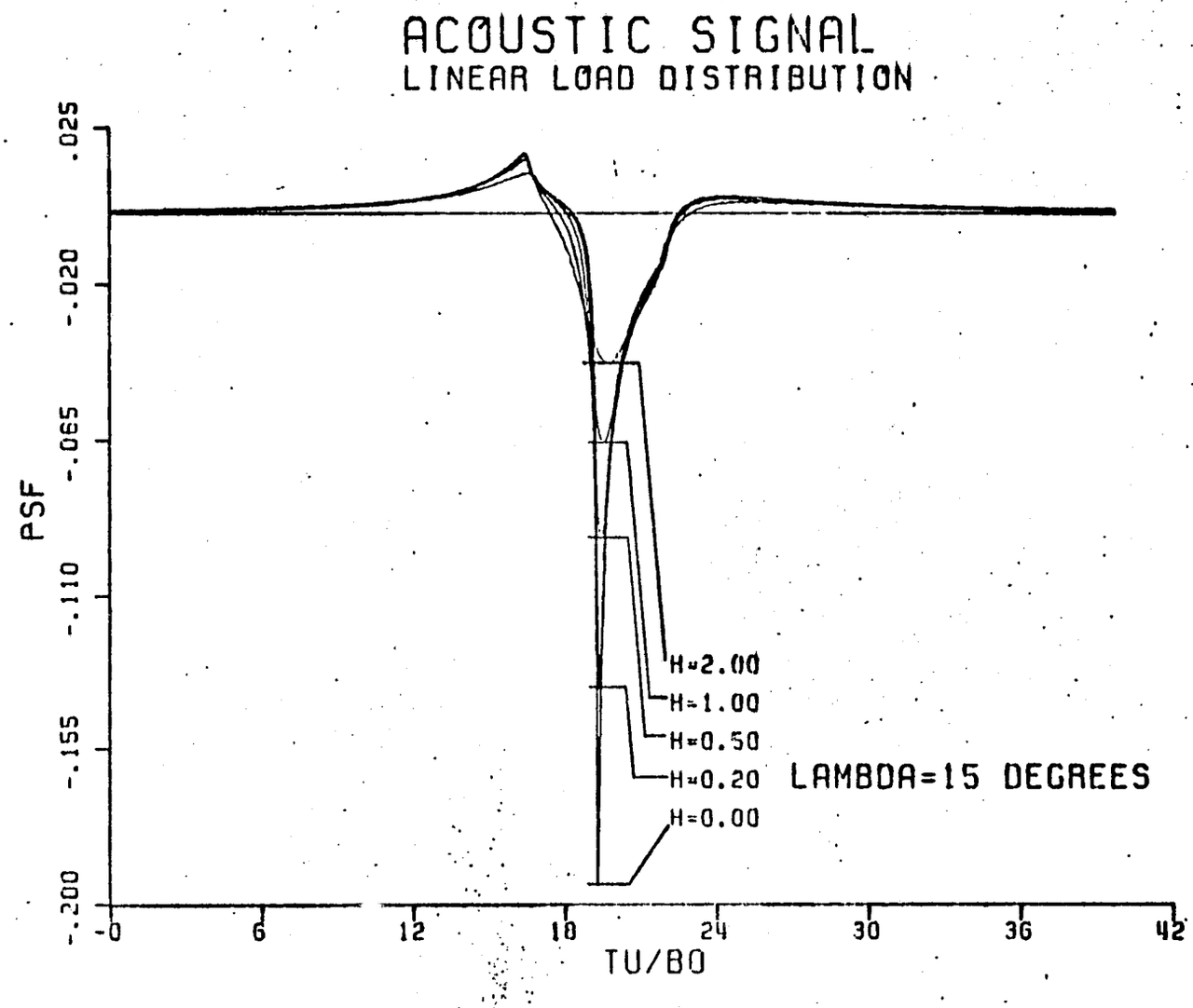
ACOUSTIC SIGNAL
LINEAR LOAD DISTRIBUTION
PSF
.025
-.020
-.065
-.110
-.155
-.200
-0
6
12
18
24
30
36
42
TU/BO
H=2.00
H=1.00
H=0.50
H=0.20
H=0.00
LAMBDA=15 DEGREES

Figure 22

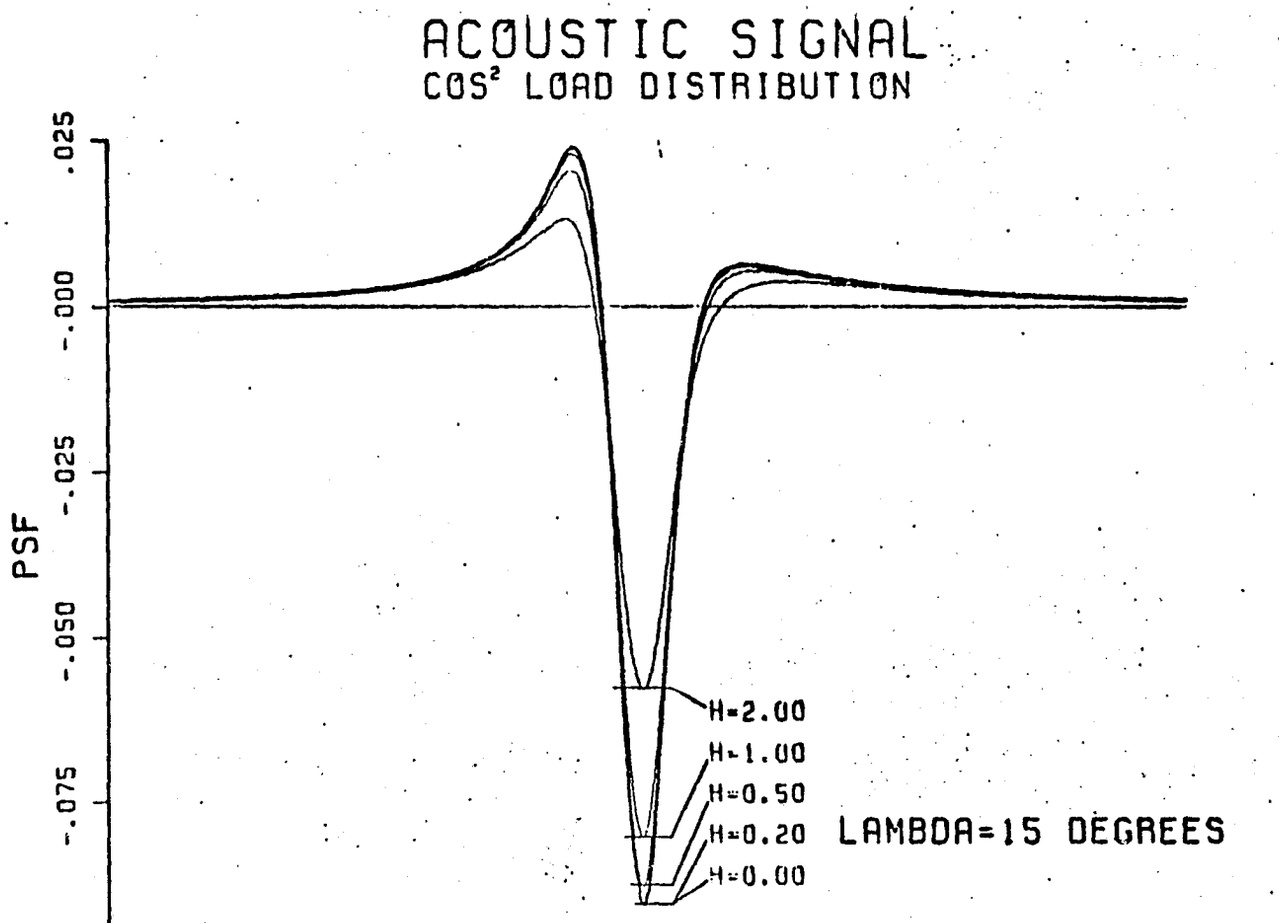
ACOUSTIC SIGNAL
COS² LOAD DISTRIBUTION
PSF
.025
-.000
-.025
-.050
-.075
-.100
-0
6
12
18
24
30
36
42
TU/BO
H=2.00
H=1.00
H=0.50
H=0.20
H=0.00
LAMBDA=15 DEGREES

Figure 23

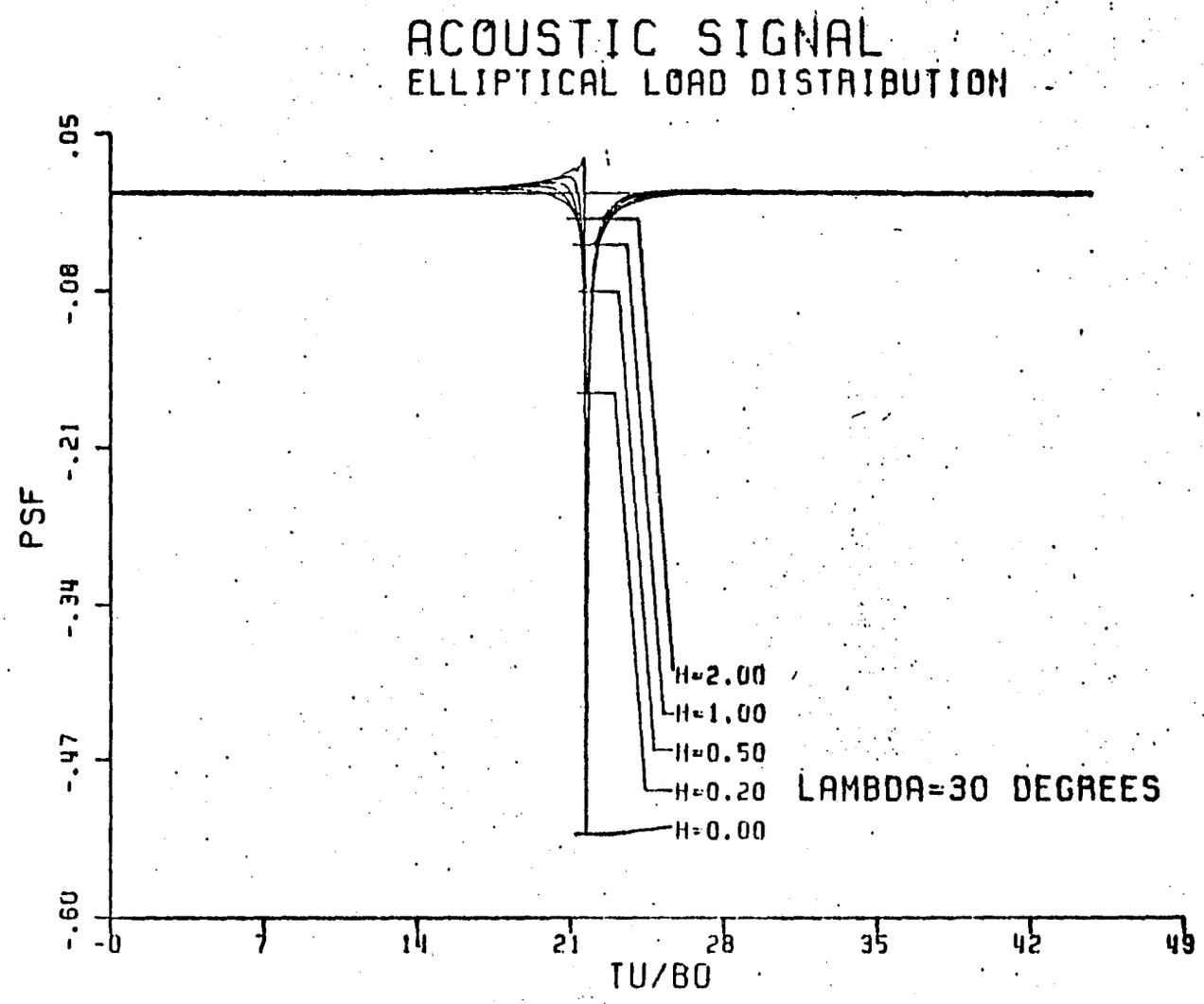
ACOUSTIC SIGNAL
ELLIPTICAL LOAD DISTRIBUTION
PSF
.05
-.08
-.21
-.34
-.47
-.60
0
7
14
21
28
35
42
49
TU/BO
H=2.00
H=1.00
H=0.50
H=0.20
H=0.00
LAMBDA=30 DEGREES

Figure 24

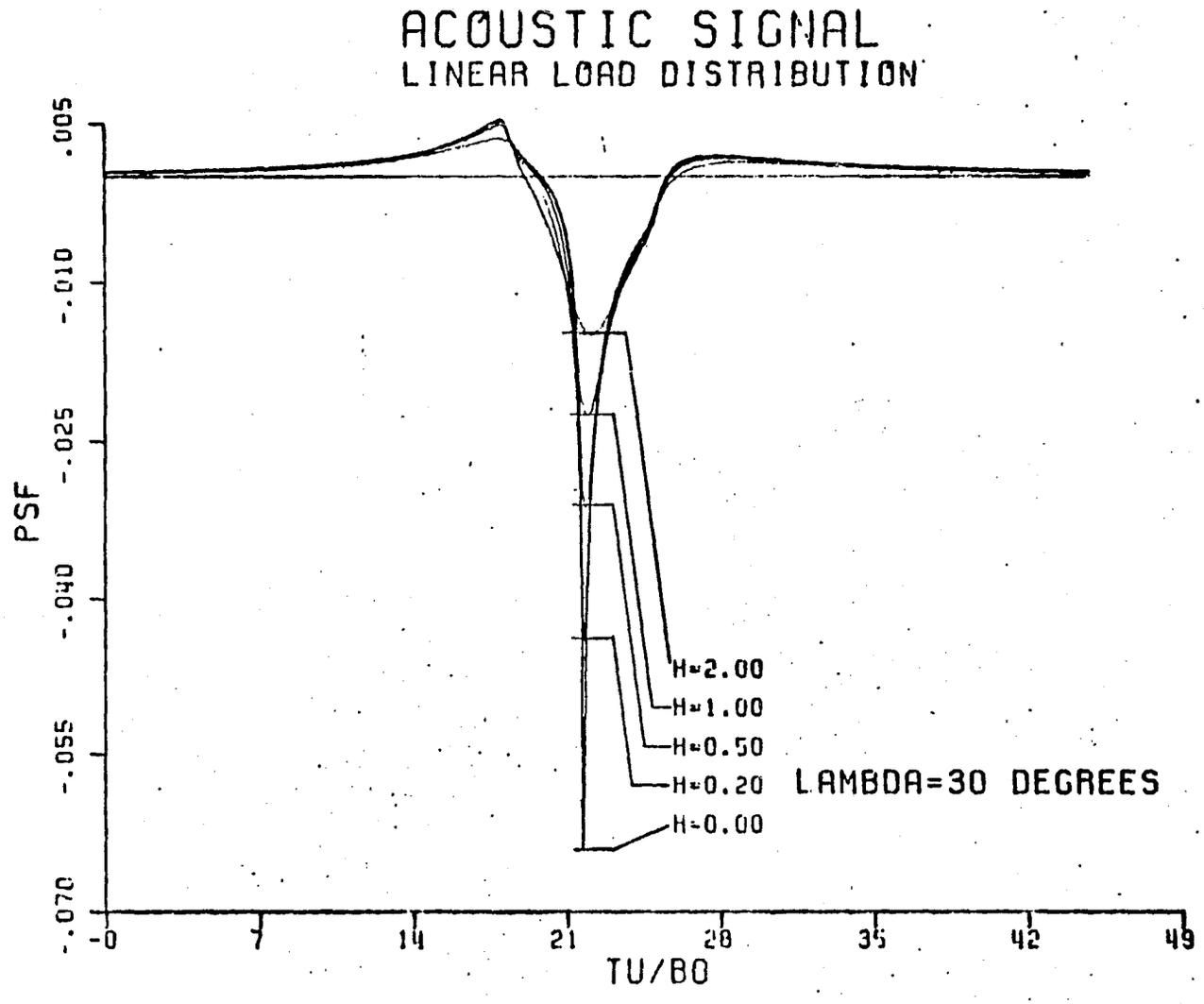
ACOUSTIC SIGNAL
LINEAR LOAD DISTRIBUTION
PSF
.005
-.010
-.025
-.040
-.055
-.070
-0
7
14
21
28
35
42
49
TU/BO
H=2.00
H=1.00
H=0.50
H=0.20
H=0.00
LAMBDA=30 DEGREES

Figure 25

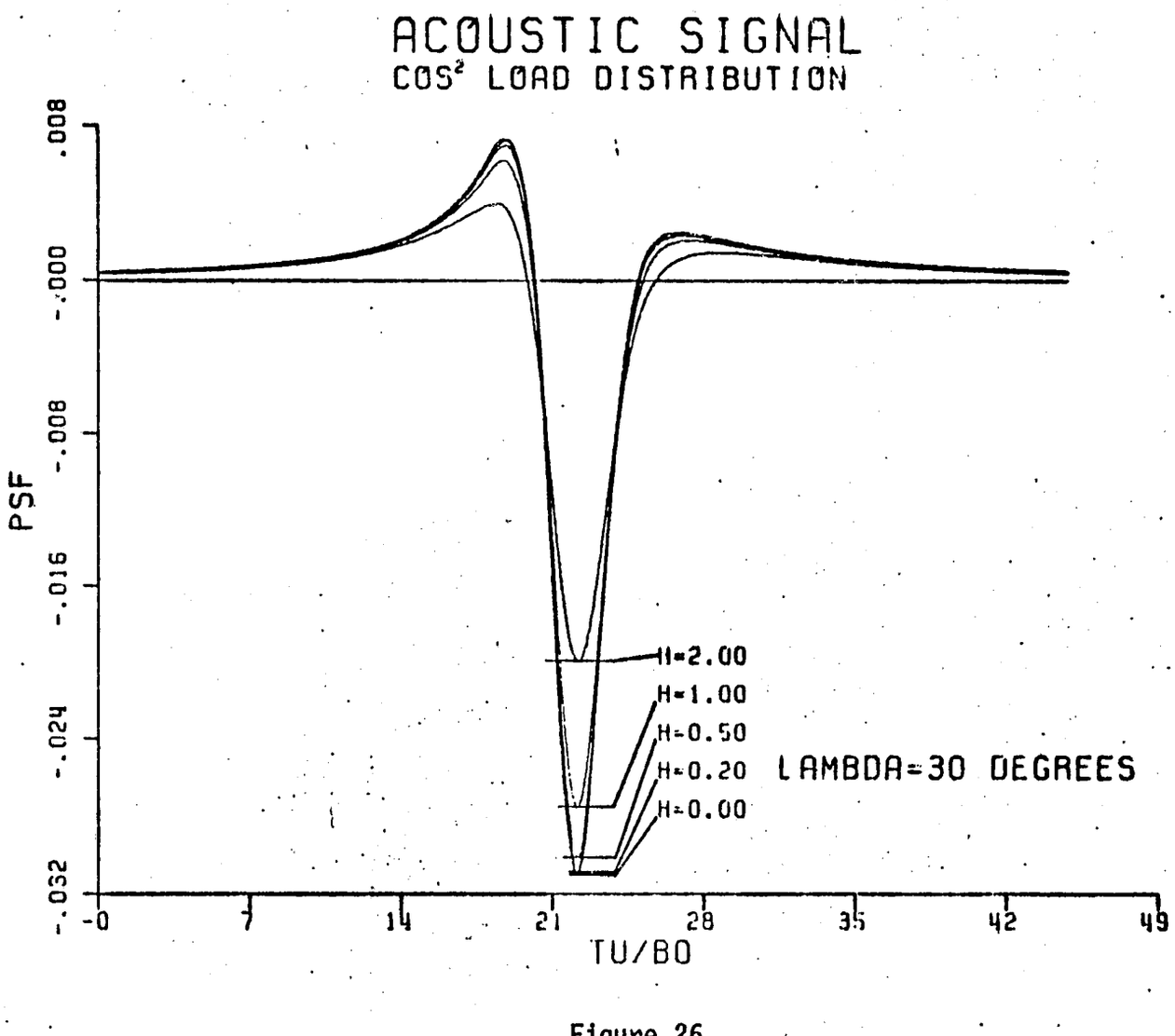
ACOUSTIC SIGNAL
COS² LOAD DISTRIBUTION
PSF
.008
-.000
-.008
-.016
-.024
-.032
-0
7
14
21
28
35
42
49
TU/BO
H=2.00
H=1.00
H=0.50
H=0.20
H=0.00
LAMBDA=30 DEGREES

Figure 26

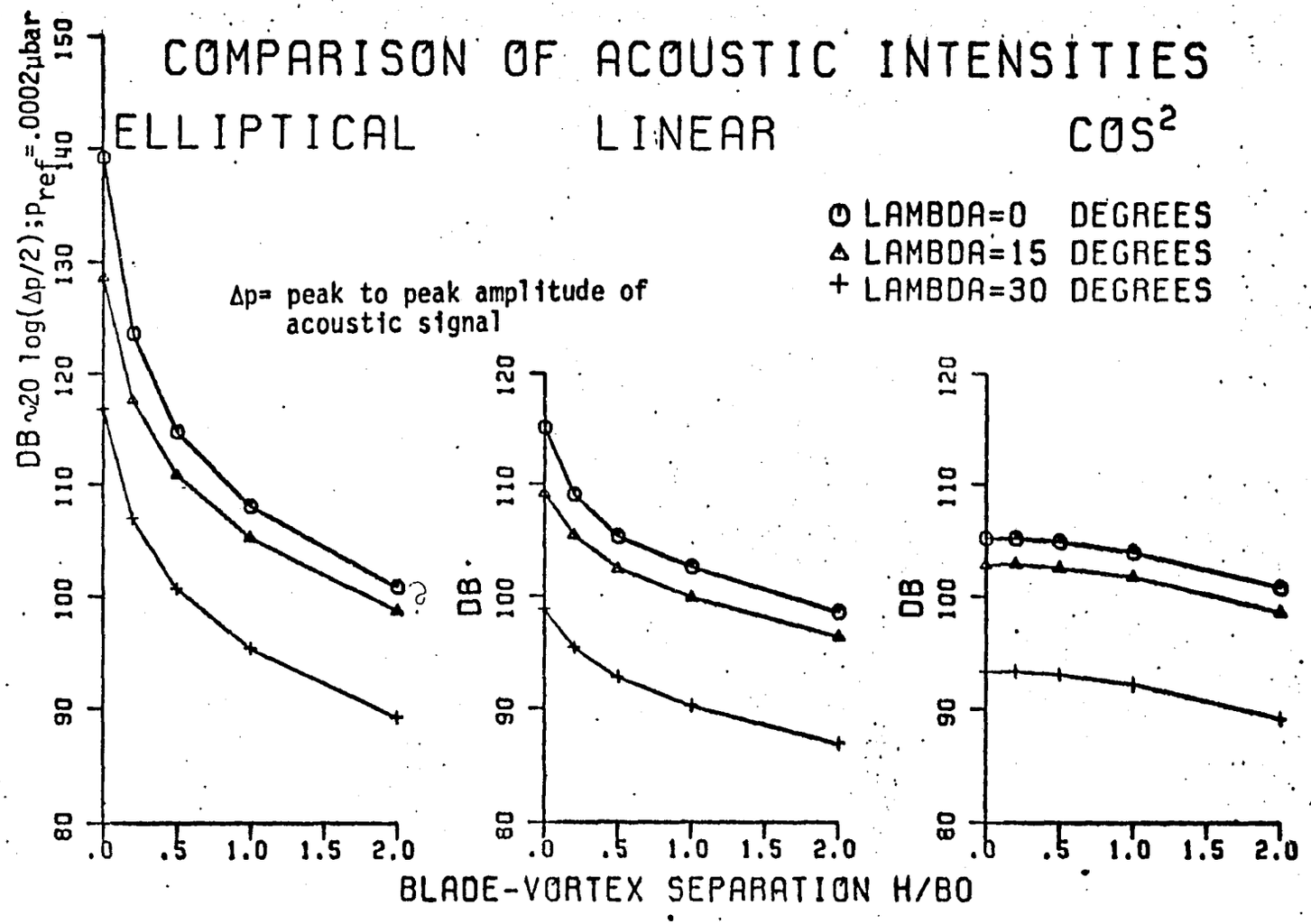
COMPARISON OF ACOUSTIC INTENSITIES
ELLIPTICAL
LINEAR
COS²
LAMBDA=0 DEGREES
LAMBDA=15 DEGREES
LAMBDA=30 DEGREES
Δp= peak to peak amplitude of acoustic signal
DB ~20 log(Δp/2):p_ref=.0002μbar
DB
80
90
100
110
120
130
140
150
.0
.5
1.0
1.5
2.0
BLADE-VORTEX SEPARATION H/BO

Figure 27

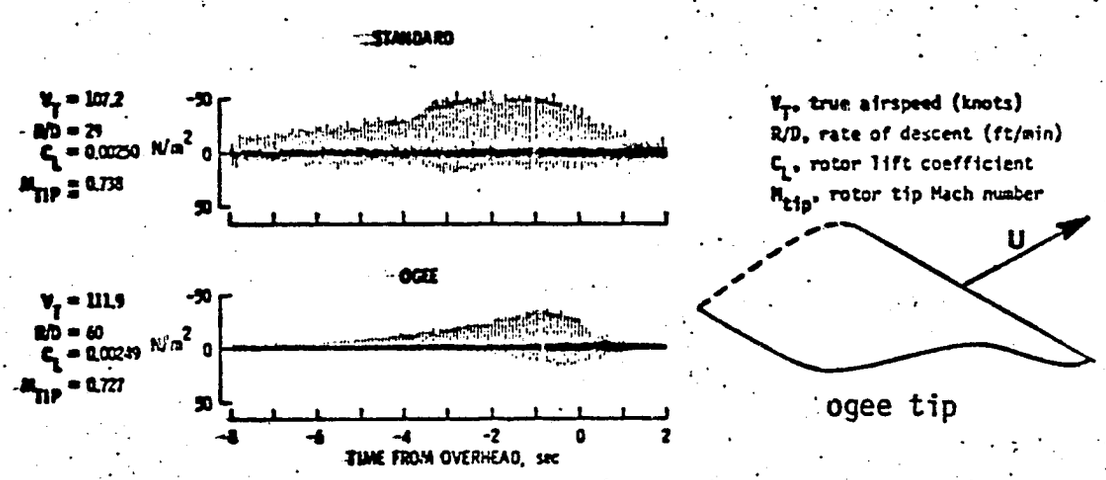

Figure 28a. Comparison of farfield acoustic signatures for ogee(fig.) and square-tipped rotor blades. Tests were conducted with a Hughes model UH-1H helicopter in level flight at a nominal 61 meter altitude. Microphone is located at ground level in line with the flight path. (ref. 8)

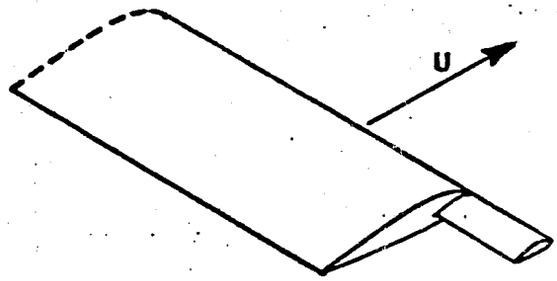

Figure 28b. Sub-wing Tip (ref. 2)

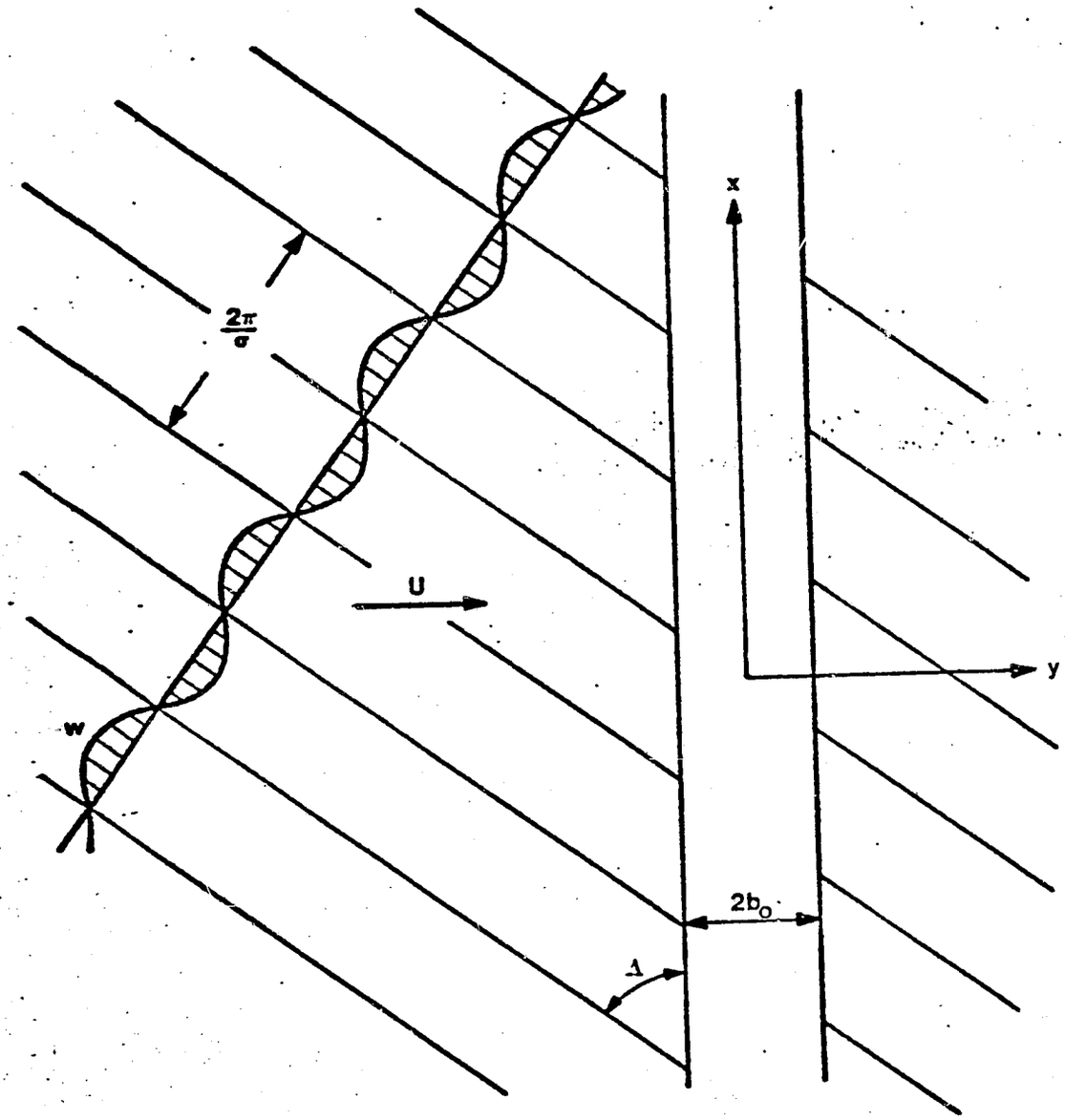

Figure B1. Infinite Span Airfoil Interacting with a sinusoidal gust (after ref. 4)

REFERENCES

1. George, A.R., "Helicopter Noise - State of the Art." AIAA Paper 77-1337, October, 1977.

2. Tangler, J.L., "The Design and Testing of a Tip to Reduce Blade Slap," Presented at the 31st Annual National Forum of the American Helicopter Society, Washington, D.C., May 1975 (Preprint 963).

3. Widnall, S.E., "Helicopter Noise Due to Blade-Vortex Interaction," The J. of the Acoustical Society of America, 50, No. 1 (part 2), pp. 354-365, 1971.

4. Chu, S., Helicopter Noise Due to Blade/Vortex Interaction, Ms. Thesis, M.I.T., June, 1971.

5. Donaldson, C.duP., Snedeker, R.S., and Sullivan, R.D., "Calculation of Aircraft Wake Velocity Profiles and Comparison with Experimental Measurements," J. of Aircraft, 11, No. 9, pp. 547-555, 1974.

6. Betz, A., NACA Tech. Memo 713, 1932.

7. Scully, M.P., Computation of Helicopter Rotor Wake Geometry and its Influence on Rotor Harmonic Airloads, Ph.D. Thesis, M.I.T., June, 1971.

8. Mantay, W.R., Shidler, P.A., and Campbell, R.L., "Some Results of the Testing of a Full-Scale Ogee Tip Helicopter Rotor; Acoustics Loads, and Performance," AIAA Paper 77-1340, October 1977.

9. Filotas, L.T., "Theory of Airfoil Response in a Gusty Atmosphere - Part I, Aerodynamic Transfer Function," UTIAS Report No. 139, University of Toronto, October, 1969.

10. Carrier, G.F., Krook, M., and Pearson, C.E., Functions of a Complex Variable, McGraw Hill, 1966, p. 272.

11. Whitham, G.B., Linear and Nonlinear Waves, John Wiley and Sons, Inc., 1973, p. 382.

12. Rossow, V.J., "On the Inviscid Rolled-Up Structure of Lift Generated Vortices," J. of Aircraft, 10, No. 11, pp. 647-650, 1973.

13. Cooley, J.W., Lewis, P.A.W., and Welch, P.D., "The Fast Fourier Transform Algorithm and its Applications," IBM Research Paper RC-1743, February 1967.

14. Boxwell, D.A., Schmitz, F.H., and Hanks, M.L., "In Flight Far-Field Measurements of Helicopter Impulsive Noise," Presented at the "First European Rotorcraft and Powered Lift Aircraft Forum," University of Southampton, Southampton, England, September 1973.

15. Amiet, R.K., "High Frequency Thin Airfoil Theory for Subsonic Flow," AIAA Journal, 14, No. 8, pp. 1076-1082, 1976.